Thermodynamic assessment of the Na-O and Na-U-O systems
Margin to the safe operation of SFRs

Smith, A. L.; Guéneau, C; Flèche, J. L.; Chatain, S.; Beneš, O.; Konings, R. J.M.

DOI
10.1016/j.jct.2017.04.003

Publication date
2017

Document Version
Final published version

Published in
The Journal of Chemical Thermodynamics

J. Chem. Thermodynamics 114 (2017) 93–115

Contents lists available at ScienceDirect

J. Chem. Thermodynamics

journal homepage: www.elsevier.com/locate/jct

Thermodynamic assessment of the Na-O and Na-U-O systems: Margin to the safe operation of SFRs

A.L. Smith [a,*], C. Guéneau [b], J.-L. Flèche [b], S. Chatain [b], O. Beneš [c], R.J.M. Konings [c]

[a] Delft University of Technology, Faculty of Applied Sciences, Radiation Science & Technology Department, Nuclear Energy and Radiation Applications (NERA), Mekelweg 15, 2629 JB Delft, The Netherlands
[b] DEN-Service de la Corrosion et du Comportement des Matériaux dans leur Environnement (SCCME), CEA, Université Paris-Saclay, F-91191 Gif-sur-Yvette cedex, France
[c] European Commission, Joint Research Centre, Directorate for Nuclear Safety & Security, P.O. Box 2340, D-76125 Karlsruhe, Germany

ARTICLE INFO

Article history:
Received 25 January 2017
Received in revised form 5 April 2017
Accepted 6 April 2017
Available online 10 April 2017

Keywords:
CALPHAD
Sodium-oxygen system
Sodium-uranium-oxygen system
Differential Scanning Calorimetry
First-principle calculations
Quasi-harmonic model

ABSTRACT

A thermodynamic model for the Na-O system was developed for the first time using the CALPHAD method after review of the structural, thermodynamic, and phase diagram data available on this system. Differential Scanning Calorimetry measurements were moreover performed to assess the phase equilibria and liquidus temperature in the Na_2O-Na_2O_2 composition range. A CALPHAD model for the Na-U-O system was furthermore developed on the basis of both reviewed experimental data, and thermodynamic functions of the sodium uranates derived by combining ab initio calculations and a quasi-harmonic statistical model. The phase equilibria in this ternary system are particularly relevant for the safety assessment of the nuclear fuel-sodium coolant interaction in Sodium-cooled Fast reactors (SFRs). The model predicts the stability of the ternary phase field UO_2-Na_3UO_4-Na_4UO_5, which is consistent with the most recent literature data. Further optimization was moreover performed to fit the sodium partial pressures measured experimentally in the $NaUO_3$-$Na_2U_2O_7$-UO_2 and $NaUO_3$-Na_2UO_4-$Na_2U_2O_7$ phase fields, yielding an overall consistent description. Finally, the oxygen content required to form pentavalent Na_3UO_4 and hexavalent Na_4UO_5 in liquid sodium at 900 K were calculated to be 0.7 and 1.5 wppm, respectively, which are levels typically encountered in SFRs.

1. Introduction

A considerable interest in the chemistry of the Na-(U,Pu)-O system has existed since the 1960s because of its technological importance for the development of Sodium-cooled Fast Reactors (SFR) [1,2]. Among the six reactor designs selected by the Generation IV International Forum (GIF), the SFR is the concept with the highest technology readiness level, and probably the first one to move to a demonstration phase and commercial deployment [1]. SFRs use liquid sodium metal as a coolant, which shows a high boiling point (1156 K), a high heat capacity, and a good thermal conductivity preventing overheating [1,2]. Some drawbacks exist with this design, however, in particular due to the chemical reactivity of sodium with water and air. The investigations reported in this work are more specifically concerned with the safety assessment of the potential interaction of the sodium metallic coolant with the nuclear fuel in the event of a breach of the stainless steel cladding. Although extremely rare, various circumstances can lead to the formation of a breach during normal operating and accidental conditions: manufacturing defaults in the cladding material, mechanical and chemical interactions between fuel and cladding material, cooling default, or unexpected change in neutron flux.

(U,Pu) O_2 mixed oxide (MOX) fuel is currently the preferred option for SFRs with a plutonium concentration of the order of 20 wt%. Past experimental work carried out in the 1980s on the reaction between liquid sodium and urania and urania–plutonia solid solutions has shown that in the temperature range of the fuel during operation, close to the pellet rim (around 893–923 K [3]), the main reaction product was Na_3MO_4 where $M = (U_{1-\alpha}Pu_{\alpha})$ [4–8]. The compound Na_3MO_4 was found to be of lower density (5.6 $g{\cdot}cm^{-3}$), and with less than half the thermal conductivity relative to the mixed oxide [9–11], leading to local swelling and temperature increase in the fuel pin. Such a situation can induce further cladding failure, restrain the flow of coolant within a subassembly of fuel pins, or result in a contamination of the primary coolant with plutonium, minor actinides, or highly radioactive fission products [9–11].

The prediction of the nature of the phases formed following the nuclear fuel-sodium coolant interaction and their compositions

* Corresponding author.
E-mail address: a.l.smith@tudelft.nl (A.L. Smith).

http://dx.doi.org/10.1016/j.jct.2017.04.003
0021-9614/

under specific temperature and oxygen potential conditions is crucial from safety perspectives. The structural properties and thermodynamic functions of the ternary phases forming in the Na-U-O phase diagram are fairly well established. Their relative stabilities and the corresponding ternary phase fields have not been investigated systematically, however, and there is no description using the CALPHAD method (CALculation of PHAse Diagrams) [12]. A sound description via models is essential, however, to feed the materials databank of computer simulation codes.

A CALPHAD model for the binary systems Na-O and Na-U as well as ternary Na-U-O system has been developed in the present study using a ionic sublattice description compatible with the already existing model for the U-O system and in general with models of the TAF-ID project [13]. The TAF-ID project has been initiated since 2013 by the OECD/NEA with the aim to develop a thermodynamic database for nuclear materials (www.oecd-nea.org/science/taf-id/) in cooperation between several countries.

A review of the structural, thermodynamic, and phase diagram data available for the Na-O system is firstly given. Differential Scanning Calorimetry measurements performed in the Na_2O-Na_2O_2 composition range are furthermore described, and the calculated phase equilibria are compared with the literature data on this system. The structural and thermodynamic properties of the ternary sodium uranates are also reviewed, and the ternary Na-U-O phase diagram is computed by extrapolation of the three constituting binary sub-systems, and further optimized. As heat capacity data are lacking at high temperatures for the sodium uranates, the corresponding thermodynamic functions are calculated by combining ab initio calculations at 0 K and a quasi-harmonic statistical model. Finally, the threshold oxygen potentials required within the fuel (or sodium coolant) to form the sodium uranate ternary phases are calculated, and compared to the typical oxygen levels encountered in SFRs.

2. Thermodynamic assessment of the Na-O system

2.1. Review of literature data

2.1.1. Phase diagram data

Wriedt made an extensive literature review of the phase diagram and thermodynamic data available on the Na-O system in 1987 [14]. Fig. 1 shows a sketch of the phase diagram published in his paper including the known boundaries, phase transformations, and three-phases equilibria. This system is poorly known, especially above 50 at% O.

Five solid phases have been reported, namely Na(cr), Na_2O(cr), Na_2O_2(cr), NaO_2(cr), and NaO_3(cr), whose crystal structures are listed in Table 1 [14].

The stable form of sodium at room temperature is body-centered cubic (bcc) β-Na(cr), in space group $Im\bar{3}m$ [14,15]. The reported measurements of the melting temperature of sodium metal are numerous and concordant. The selected value, i.e., $T_{fus}(Na, cr) = (370.98 \pm 0.02)$ K was taken from [24].

Sodium oxide, Na_2O, shows a cubic phase at room temperature, in space group $Fm\bar{3}m$ [14,16]. Bouaziz et al. observed two phase transitions at 1023 and 1243 K, respectively, when performing differential thermal analysis (DTA) measurements on a very high-purity sample [25]. The existence of those phase transitions is subject of controversy, however. Henry et al. [26] could not reproduce the same results by DTA, while Maupre [27] could only observe them on cooling after fusion of the sodium oxide [14]. Wriedt chose not to include them in his description of the binary system (Fig. 1) [14]. The melting point of sodium oxide was determined at $T_{fus}(Na_2O, cr) = (1405.2 \pm 4)$ K by Bouaziz et al. [24,25]. Finally, Na_2O is expected to possess a very limited hypo- and hyper-stoichiometric homogeneity range [14]. It was therefore treated as a stoichiometric compound in the present thermodynamic model.

Sodium peroxide, Na_2O_2, exhibits two polymorphs with a phase transition at 785 K, as determined in the X-ray diffraction studies of Tallman and Margrave [18,28]. A third polymorph was prepared by quenching Na_2O_2 in liquid air, but is not stable at room temperature [14]. Na_2O_2-I is hexagonal, in space group $P\bar{6}2m$ [17], but the crystal structure of Na_2O_2-II was not reported. Na_2O_2-II melts at $T_{fus}(Na_2O_2, cr) = 948$ K [18,24,29]. Some evidence for the existence of a hypostoichiometric Na_2O_{2-x} homogeneity range was reported in the literature. This domain is very narrow below 573 K, but can reach $Na_2O_{1.95}$ and possibly $Na_2O_{1.67}$ above 773–873 K [14,29,30]. The data available are too limited to define accurately its shape, however. The hypostoichiometry of sodium peroxide was therefore not treated in the present thermodynamic model.

Sodium superoxide, NaO_2, has a cubic structure at room temperature [14,21]. Two structural transitions to NaO_2-II and NaO_2-III, and a magnetic ordering transition to NaO_2-IV were observed below room temperature. The melting point of NaO_2-I was found at $T_{fus}(NaO_2 - I, cr) = (825 \pm 10)$ K [14,24]. NaO_2-I is not thermally stable. It reaches the $NaO_{1.8}$ composition when heated at (548 ± 25) K, following a decomposition reaction to sodium peroxide and oxygen [14,30].

Finally, the crystal structure of sodium ozonide, NaO_3, was identified in 1964 as tetragonal in space group $I4/mmm$ for a sample prepared by the reaction of ozone with sodium hydroxide [14,31]. More recently, Klein *et al.* have synthesized NaO_3 from cesium ozonide using cation exchange in liquid ammonia [22,23]. After addition of dimethyl amine to the sodium ozonide solution in ammonia and solvent evaporation below 253 K, the authors obtained a pure bright red microcrystalline powder. They showed NaO_3 to be isostructural with sodium nitrite $NaNO_2$, i.e., tetragonal in space group $Im2m$ [22,23]. The authors moreover reported NaO_3 to decompose slowly at room temperature into solid NaO_2 and oxygen. Rapid spontaneous decomposition occurs at 310 K. No thermodynamic data are available on this phase, except for an estimated value of the enthalpy of formation [14,32]. As NaO_3 appears not to be stable at room temperature, it was not included in the CALPHAD assessment.

Liquidus data were reported by Bunzel et al. on the O-rich side of Na_2O and O-deficient side of Na_2O_2 [14,29]. The authors interpreted them incorrectly, however, and Wriedt proposed a revised representation of the phase diagram as depicted in Fig. 1.

The knowledge of the oxygen solubility limit in liquid sodium is of great technological importance for Sodium-cooled Fast Reactors as the oxygen dissolved in liquid sodium causes the corrosion of the materials with which it is in contact [14]. The experimental studies have been numerous, but the literature shows rather large inconsistencies with very different oxygen solubility equations reported [14,33–37]. The one selected herein, and recommended in the paper of Wriedt [14], is from the work of Noden who reviewed critically all the data reported in the literature and fitted 268 recommended experimental points from twelve investigators with a least square method between 377 and 873 K [36,37]: $\log[C_O(\text{wppm})] = 6.2571 - 2444.5/T$. The author discarded, however, the results obtained from mercury amalgamation methods below about 523 K due to large blank errors. The derived equation is in very good agreement with a previous review by Eichelberg [33] based on 107 selected values, which discarded the amalgamation data and that obtained in glassware: $\log[C_O(\text{wppm})] = 6.239 - 2447/T$. It differs rather largely, however, from the review of Claxton [34,35], based on 88 experimental points, but not discarding any of them:

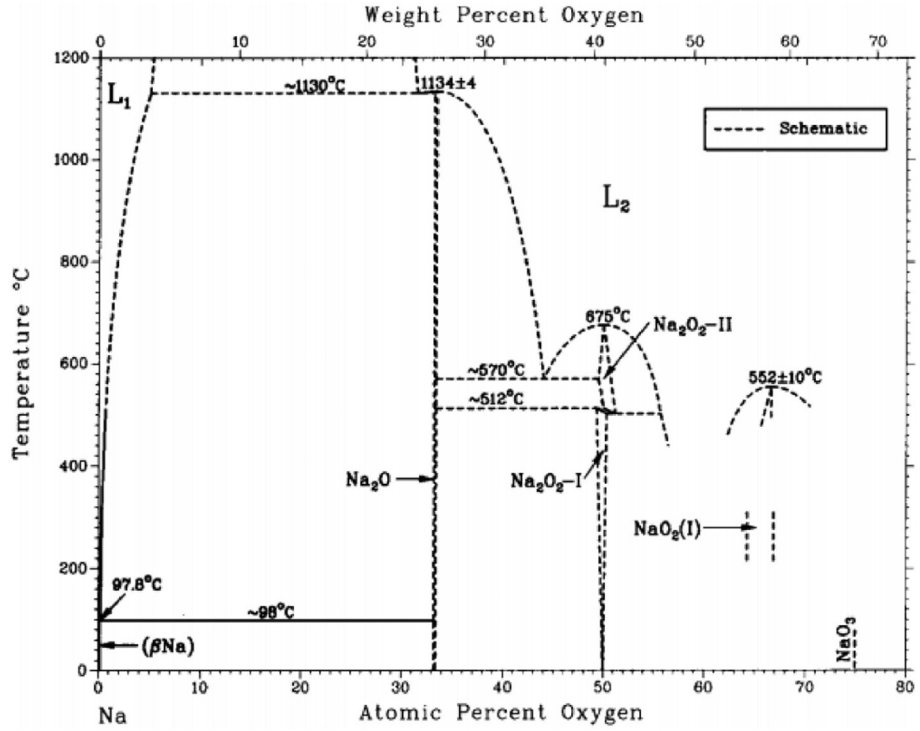

Fig. 1. Sketch of the Na-O phase diagram published in the paper of Wriedt [14], reproduced with permission by Springer.

Table 1
Summary of the crystal structures and lattice parameters in the Na-O system at (0.10 ± 0.01) MPa. RT = (295 ± 2) K.

Phase	Symmetry	Space group	Lattice parameters/nm	T/K	Ref.
β-Na (bcc)	cubic	$Im\bar{3}m$	a = 0.428865[a]	RT	[14,15]
Na_2O-I	cubic	$Fm\bar{3}m$	a = 0.555	RT	[14,16]
Na_2O-II	–	–	–	–	
Na_2O-III	–	–	–	–	
Na_2O_2-I	hexagonal	$P\bar{6}2m$	a = 0.6207[b], c = 0.4471[b]	RT	[14,17,18]
Na_2O_2-II	–	–	–	–	
NaO_2-IV	orthorhombic	$Pnnm$	a = 0.4335, b = 0.5537, c = 0.3363	4	[14,19]
NaO_2-III	orthorhombic	$Pnnm$	a = 0.426, b = 0.554, c = 0.344	173	[14,20]
NaO_2-II	cubic	$Pa\bar{3}$	a = 0.546[c]	203	[14,20]
NaO_2-I	cubic	$Fm\bar{3}m$	a = 0.5512[d]	293	[14,19,21]
NaO_3	tetragonal	$Im2m$	a = 0.35070[e], b = 0.57703[e], c = 0.52708[e]	213	[22,23]

Standard uncertainties u are [a] $u(a)$ = 0.000026 nm.
Standard uncertainties u are [b] $u(a)$ = 0.0004 nm, $u(c)$ = 0.0003 nm.
Standard uncertainties u are [c] $u(a)$ = 0.001 nm.
Standard uncertainties u are [d] $u(a)$ = 0.002 nm.
Standard uncertainties u are [e] $u(a)$ = 0.00002 nm, $u(b)$ = 0.00003 nm, $u(c)$ = 0.00003 nm.

$\log[C_O(\text{wppm})] = 5.21 - 1777/T$. For comparison the equations suggested by Noden [36,37], Eichelberg [33], and Claxton [34,35] are shown in the phase diagram in Fig. 7.

2.1.2. Thermodynamic data

The thermodynamic functions of sodium metal and its oxides used for the CALPHAD model are summarized in Tables 2 and 3. Those were taken from the critical reviews and compilations of [14,24,38–43]. A detailed description of the available literature data for these phases can be found in [14,24,42].

The standard entropy of β-Na(cr) was taken from the CODATA key values [38], based on the low temperature heat capacity measurements of Martin and Filby [44,45]. The enthalpy of fusion selected herein and in the review work of [42] is based on the work of Martin [46]. The heat capacity functions of Na(cr) and Na(l) used for the thermodynamic model are those of Dinsdale [40].

Very different values have been reported for the enthalpy of formation of Na_2O(cr) due to the presence of impurities in the investigated samples. The value derived by O'Hare [47], who gave a specific attention to the compound's purity, is $-(414.82 \pm 0.28)$ kJ·mol^{-1}. The latter value differs rather significantly, however, from that selected in the JANAF compilation [24], i.e., $-(417.98 \pm 4.2)$ kJ·mol^{-1}. The data selected herein was taken from the compilation of Knacke [39], i.e., $-(415.1 \pm 4.2)$ kJ·mol^{-1}, which is in good agreement with the data of O'Hare. The standard entropy adopted in the JANAF compilation and in this work is based on unpublished measurements by Furukawa [48] after correction for Na_2CO_3(cr) impurities [24]. The choice of the heat capacity function for sodium oxide Na_2O requires a more detailed discussion. The heat capacity function selected herein was taken from the compilation of JANAF [24], which is based on the enthalpy increment data of Grimley and Margrave, collected between 380.1 and

Table 2
Summary of thermodynamic data for pure elements and oxides selected in the present work.

Phase	$\Delta_f H^o_m(298.15\ K)$/ (kJ·mol^{-1})	$\Delta_{tr} H^o_m(T_{tr})$/ (kJ·mol^{-1})	$\Delta_{fus} H^o_m(T_{fus})$/ (kJ·mol^{-1})	$S^o_m(298.15\ K)$/ (J·K^{-1}·mol^{-1})
β-Na(cr)	0	–	–	51.3 ± 0.2 [38,40,43]
Na(l)	–	–	2.598 ± 0.005 [39,41,42]	
Na_2O-I(cr)	−415.1 ± 4.2 [39]	–	–	75.04 ± 0.10 [24,42]
Na_2O-II(cr)	–	1.757 [24]	–	–
Na_2O-III(cr)	–	11.924 [24]	–	–
Na_2O(l)	–	–	47.7 ± 2.5 [24,25]	–
Na_2O_2-I(cr)	−513.21 ± 5.0 [24,39]	–	–	94.809 ± 1.3 [24,39]
Na_2O_2-II(cr)	–	5.732 [24,39]	–	–
Na_2O_2(l)	–	–	24.518 [39]	–
NaO_2-I(cr)	−260.66 ± 2.9 [24]	–	–	115.90 ± 1.3 [24]
NaO_3(cr)	−188 [14,32]	–	–	–

The reported uncertainties correspond to standard uncertainties.

Table 3
Summary of heat capacity data for pure elements and oxides selected in the present work.

Phase	$C_{p,m}=A+B\cdot T+C\cdot T^2+E\cdot T^{-2}$/J·K^{-1}·mol^{-1}				Temp. range/K
	A	B	C	E	
β-Na(cr)	51.03936	$-14.46133\cdot10^{-2}$	$2.618297\cdot10^{-4}$	−264307.5 [40]	298–370.9
Na(l)	38.11988	$-19.49171\cdot10^{-3}$	$1.023984\cdot10^{-5}$	−68684.96 [40]	370.9–3000
Na_2O-I(cr)	66.216	$43.865\cdot10^{-3}$	$-1.4088\cdot10^{-5}$	−813400 [24]	298–1023.2
Na_2O-II(cr)	66.216	$43.865\cdot10^{-3}$	$-1.4088\cdot10^{-5}$	−813400 [24]	1023.2–1243.2
Na_2O-III(cr)	66.216	$43.865\cdot10^{-3}$	$-1.4088\cdot10^{-5}$	−813400 [24]	1243.2–1405.2
Na_2O(l)	104.6 [24]				1405.2–3000
Na_2O_2-I(cr)	80.965	$62.463\cdot10^{-3}$	$-2.2004\cdot10^{-5}$	−746400 [24,39]	298.15–785
Na_2O_2-II(cr)	113.596 [24,39]				785–948
Na_2O_2(l)	117.15 [39]				948–3000
NaO_2-I(cr)	59.953	$40.853\cdot10^{-3}$ [24]	–		298.15–825

1174.6 K using a copper block drop calorimeter [49]. The data of [49] measured in the range 380.1–980.4 K were extrapolated up to the melting point, taking into account the two phase transitions and heats of transitions determined by Bouaziz et al. [25]. The reported enthalpy data above 1078.3 K were considered too large, however, and therefore unreliable [24]. Fredrickson and Chasonov also performed enthalpy increment measurements using drop calorimetry in 1973, but failed to identify any phase transition up to 1300 K [50]. The authors observed a sharp rise in the heat capacity above 900 K, however, which they explained by the onset of a diffuse transition in Na_2O and a disordering of Na^+ cations. Those measurements were preferred in the review of Pankratz [51]. The enthalpy increment and heat capacity functions calculated with the present thermodynamic model are shown in Figs. 2a and b and compared with the literature data. Finally, the transition enthalpies and enthalpy of fusion of Na_2O are that selected in the JANAF compilation [24] based on the measurements of Bouaziz et al. [25].

The enthalpy of formation of sodium peroxide retained in the JANAF compilation and herein is based on the work of Gilles and Margrave [52] on a high purity sample, while the selected standard entropy is based on the low temperature heat capacity measurements of Todd [53] after correction for Na_2CO_3(cr) impurities. The heat capacity function used in the model is again that of the JANAF compilation, which was derived from the enthalpy increment measurements by Chandrasekharaiah using drop calorimetry [54]. The latter data suggested the existence of a transition between 773 and 793 K, in good agreement with the high

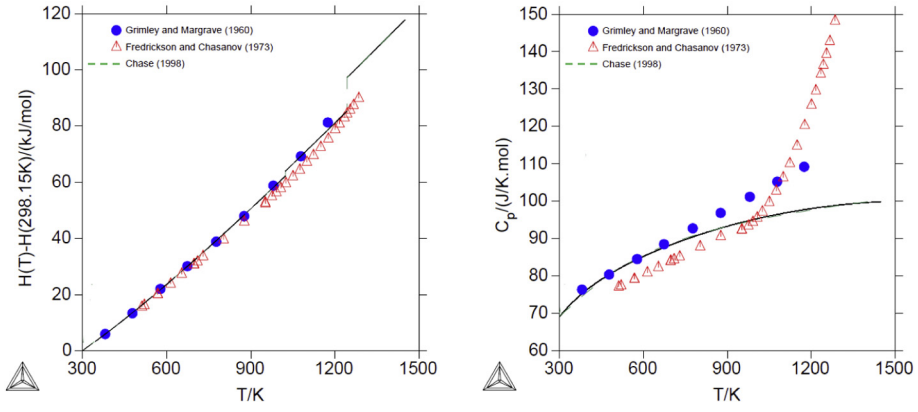

Fig. 2. (a) Calculated enthalpy increment and (b) heat capacity of sodium oxide Na_2O as a function of temperature (plain lines), and comparison with the literature data.

temperature X-ray diffraction and thermal analysis measurements of Tallman and Margrave [28]. The enthalpy of fusion of sodium peroxide is unknown [24]. It was estimated in the compilation of [39].

Finally, the thermodynamic data of sodium superoxide used in the model were taken from the JANAF compilation. The enthalpy of formation was measured by Wagman [55], the low temperature heat capacity and hence standard entropy by Todd [53], while only estimated values were reported for the enthalpy increments and heat capacity at high temperatures [24].

2.1.3. Vapour pressure studies

The gas phase in equilibrium with condensed and liquid Na was found to be composed of the monomer, dimer [14], and possibly very low concentrations of tetramer [14]. Sodium oxide vaporizes according to the following decomposition mechanisms [56,57]:

$$Na_2O(cr) = 2Na(g) + \frac{1}{2}O_2(g) \quad (1)$$

$$Na_2O(cr) = Na_2O(g) \quad (2)$$

$$Na_2O(cr) = NaO(g) + Na(g) \quad (3)$$

At any temperature, the resulting congruent vaporizing composition of sodium oxide imposed by effusion becomes $Na_{2+x}O$(cr) with the associated vaporization reaction [58]:

$$2Na_{2+x}O(cr) = 2Na(g) + \frac{1}{2}(1-2x)O_2(g) + Na_2O(g) + 2xNaO(g) \quad (4)$$

The value of x is very small, however, as sodium oxide has a very narrow homogeneity range [14]. This implies that the main gaseous species above Na_2O(cr) are Na(g), O_2(g) and Na_2O(g), the latter species being a minor vapour constituent [56,59]. The gas phase used for this work therefore considers only the species Na (g), Na_2(g), Na_2O(g), O(g), O_2(g), and O_3(g).

2.2. Differential Scanning Calorimetry measurements

2.2.1. Materials and method

Differential Scanning Calorimetry (DSC) measurements were performed with a SETARAM MDHTC96 apparatus in an attempt to gain a better insight into the poorly described liquidus line between Na_2O and Na_2O_2.

The materials investigated were sodium peroxide (Na_2O_2, >95%, Sigma–Aldrich) and sodium peroxide/sodium metal mixtures (Na, 99.95% trace metal basis, Sigma–Aldrich) (Table 4), which were handled exclusively in the dry atmosphere of an argon-filled glove box because of their hygroscopic nature and reactivity with water and air. They were moreover placed in a boron nitride liner and encapsulated for the calorimetric measurements in stainless steel crucibles closed with a screwed bolt as described in [60] to avoid vaporization and to prevent any contact with air and atmospheric water. Boron nitride was found the most suitable liner material for these investigations. Nickel, platinum, and graphite liners were also tested, but found to react with the sodium compounds.

The measurement program consisted in four successive heating cycles with 10 K/min heating rate, and 5–7-10–15 K/min cooling rates. The DSC is equipped with a furnace and a detector monitoring the difference in heat flow between sample and reference crucible. The temperatures were monitored throughout the experiment by a series of interconnected S-types thermocouples. The temperature on the heating ramp was calibrated by measuring the melting points of standard materials (Au, Ag, In, Al, Pb, Sn, Zn, Cu). The temperature on the cooling ramp was obtained by extrapolation to 0 K/min cooling rate. In both cases the melting and solidification temperatures were derived as the onset temperature using tangential analysis of the recorded heat flow. The same analysis was performed for sodium peroxide and mixtures in the Na_2O-Na_2O_2 pseudo-binary section. In this case, the transition, eutectic and melting temperatures were derived on both heating and cooling ramps as the onset temperature, while liquidus equilibria were taken as the offset on the heating ramp, and onset on cooling ramp. The uncertainty on the derived transition temperatures is estimated at about 5 K for the pure compound and 10 K for the mixtures.

The sodium peroxide material was measured up to 1073 K. A typical example of the output of the measurement is shown in Fig. 3. The first small endothermic peak corresponds to the Na_2O_2-I→Na_2O_2-II phase transition, while the second intense endothermic peak is the melting of Na_2O_2-II.

The measurements of the sodium peroxide/sodium metal mixtures were carried out up to 1373 K. The first heating cycle allowed mixing and reaction of the initial products to a specific composition point between sodium oxide and sodium peroxide as written in Eq. (5) with x between 0 and 1:

$$xNa(cr) + \frac{2-x}{2}Na_2O_2(cr) = Na_2O_{2-x}(cr) \quad (5)$$

The first cycle was not considered for the analysis. A typical example of the output obtained for the $Na_2O_{1.8}$ composition ($0.2Na + 0.9Na_2O_2$) is shown in Fig. 4. The first peak corresponds to the Na_2O_2-I→Na_2O_2-II transition and the second peak to an eutectic equilibrium. The interpretation for the third feature is not straigthforward (Na_2O-I→Na_2O-II transition or liquidus?), however, as detailed in Section 2.4.

2.2.2. DSC results

The temperatures derived from those measurements are listed in Table 5 together with their associated equilibria. The Na_2O_2-I→Na_2O_2-II transition temperatures recorded herein, i.e., (756.8 ± 5) K and (765.8 ± 10) K, are lower than determined by Tallman and Margrave using X-ray diffraction, i.e., (785 ± 1) K. The uncertainty on our measurement is large, however, considering the very small heat flow areas of the corresponding peaks. The melting point is in rather good agreement with the value of Bunzel [29]. The results obtained with the sodium peroxide/sodium metal mixtures are discussed in Section 2.4 together with the thermodynamic model developed in this work.

2.3. Thermodynamic modelling of the binary Na-O system

Only the parameters of the liquid phase were optimized in this work. Na_2O, Na_2O_2 and NaO_2 were treated as stoichiometric compounds. The Gibbs energy functions of all the phases are referred

Table 4
Provenance and purity of the samples used in this study.

Formula	Source	State	Color	Mass fraction purity*
Na_2O_2	Sigma–Aldrich	Powder	White	>0.95 ± 0.005
Na	Sigma–Aldrich	Ingot	Grey	0.9995 ± 0.0005

* The quoted uncertainties correspond to standard uncertainties.

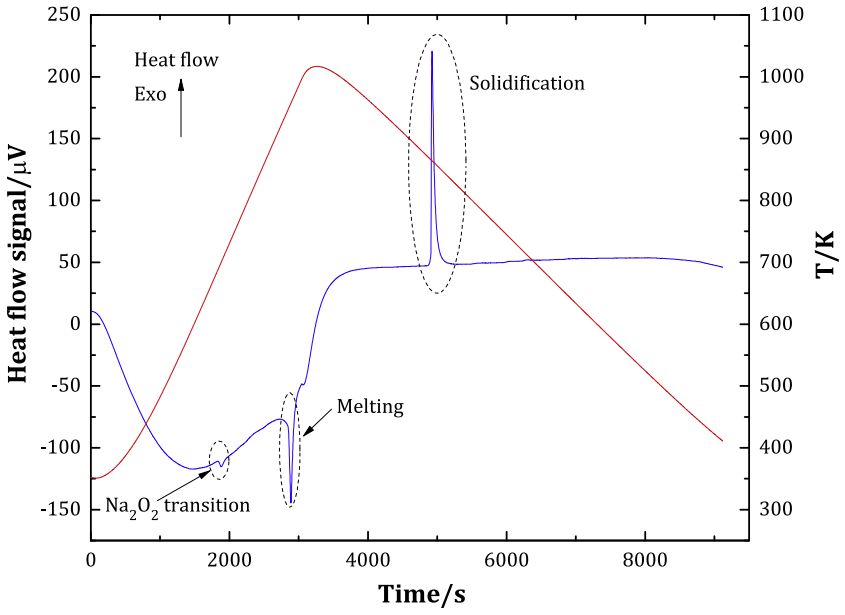

Fig. 3. Example of the DSC output for one heating cycle of the sodium peroxide material.

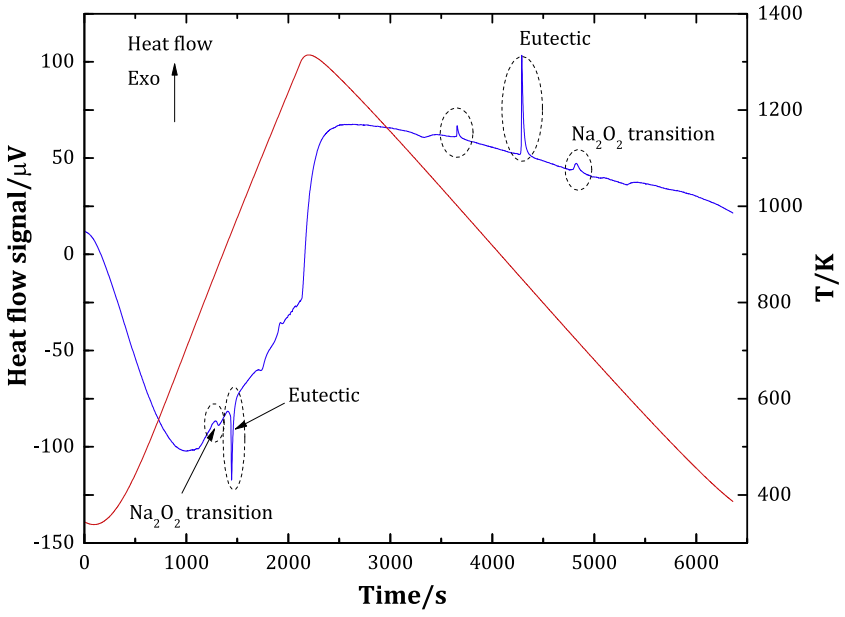

Fig. 4. Example of the DSC output for one heating cycle of the sodium peroxide/sodium metal mixture with $Na_2O_{1.8}$ composition.

Table 5
Transition temperature data in the Na-O system obtained by DSC. Data were measured under argon flow at a pressure of (0.105 ± 0.005) MPa. [H] = Data obtained on the heating ramp, [C] = Data obtained on the cooling ramp.

Sample composition x(O)	Transition type	Reaction	T/K	Cycle*
0.5	Polymorphic	Na_2O_2-I = Na_2O_2-II	756.8[a]	[H]
	Congruent melting	Na_2O_2-II = L2	939.8[a]	[H]
0.4737	Polymorphic	Na_2O_2-I = Na_2O_2-II	765.8[b]	[C]
	Eutectic	L2 = Na_2O-I + Na_2O_2-II	863.5[b]	[C]
	Polymorphic	Na_2O-I = Na_2O-II	991.6[b]	[C]
0.4594	Eutectic	L2 = Na_2O-I + Na_2O_2-II	832.6[b]	[C]
	Polymorphic	Na_2O-I = Na_2O-II	1042.8[b]	[C]
0.4286	Eutectic	L2 = Na_2O-I + Na_2O_2-II	821.2[b]	[C]
	Polymorphic	Na_2O-I = Na_2O-II	1025.5[b]	[C]
0.375	Eutectic	L2 = Na_2O-I + Na_2O_2-II	819.7[b]	[C]

Standard uncertainties u are [a]u(T) = 5 K, [b]u(T) = 10 K.

to the enthalpy of the pure elements in their stable state at room temperature 298.15 K and 1 bar ($^{o}H_i^{SER}$(298.15 K)).

2.3.1. Pure elements

The Gibbs energy functions of the pure elements *i* at temperature T and in their state φ are given by:

$$G_i^{\varphi}(T) - {}^{o}H_i^{SER}(298.15\ \mathrm{K}) = a + b\cdot T + c\cdot T\cdot lnT + \sum d_n T^n \quad (6)$$

where *n* is an integer (2, 3, −1…). In the present work, the parameters reported by Dinsdale [40] were used for pure sodium and oxygen, respectively.

2.3.2. Stoichiometric compounds

The Na_2O, Na_2O_2 and NaO_2 oxides were described with the two-sublattice model. The corresponding Gibbs energy functions have the same form as in Eq. (6):

$$G^{\varphi}(T) - \sum_i n_i^{\varphi}\,{}^{o}H_i^{SER}(298.15\ \mathrm{K}) = a + b\cdot T + c\cdot T\cdot lnT + \sum d_n T^n \quad (7)$$

where n_i^{φ} is the number of atoms of the *i*th element in the oxide formula. The coefficients *a*, *b*, *c* and d_n were calculated using the thermodynamic functions listed in Tables 2 and 3.

2.3.3. Liquid phase

The ionic two-sublattice model was used to describe the liquid phase [61], with Na^+ cations on the first sublattice, and O^{2-} anions, charged vacancies Va^{Q-}, neutral sodium peroxide Na_2O_2, and oxygen O on the second sublattice:

$$(Na^+)_P(O^{2-}, Na_2O_2, Va^{Q-}, O)_Q \quad (8)$$

P and *Q* are equal to the average charge of the opposite sublattice:

$$Q = 1$$
$$P = y_{Va^{Q-}} + 2y_{O^{2-}} \quad (9)$$

where $y_{Va^{Q-}}$ and $y_{O^{2-}}$ are the site fractions of vacancies and divalent oxygen ions on the second sublattice. The induced charge of the vacancies corresponds to the average charge of the cation sublattice, i.e., $Q = 1$, while *P* varies with the composition via the site fractions $y_{O^{2-}}$ and $y_{Va^{Q-}}$ so as to keep the phase electrically neutral.

The Gibbs energy of the liquid phase is given by the following expression:

$$\begin{aligned} G^{liquid} =& y_{O^{2-}}\cdot{}^{o}G_{(Na^+)_2(O^{2-})_1} + y_{Na_2O_2}\cdot{}^{o}G_{Na_2O_2} + y_{Va^{Q-}}\cdot{}^{o}G_{(Na^+)_1(Va^{Q-})_1} + y_O\cdot{}^{o}G_O \\ &+ QRT(y_{O^{2-}} lny_{O^{2-}} + y_{Na_2O_2} lny_{Na_2O_2} + y_{Va^{Q-}} lny_{Va^{Q-}} + y_O lny_O) \\ &+ y_{O^{2-}}y_{Va^{Q-}}[L^0_{(Na^+)_P(O^{2-},Va^{Q-})_Q} + (y_{Va^{Q-}} - y_{O^{2-}})L^1_{(Na^+)_P(O^{2-},Va^{Q-})_Q} \\ &+ (y_{Va^{Q-}} - y_{O^{2-}})^2 L^2_{(Na^+)_P(O^{2-},Va^{Q-})_Q}] + y_{O^{2-}}y_{Na_2O_2}L^0_{(Na^+)_P(O^{2-},Na_2O_2)_Q} \\ &+ y_{Na_2O_2}y_O[L^0_{(Na^+)_P(Na_2O_2,O)_Q} + (y_{Na_2O_2} - y_O)L^1_{(Na^+)_P(Na_2O_2,O)_Q}] \end{aligned} \quad (10)$$

where ${}^{o}G_{(Na^+)_2(O^{2-})_1}$, ${}^{o}G_{Na_2O_2}$, ${}^{o}G_{(Na^+)_1(Va^{Q-})_1}$, and ${}^{o}G_O$ are the reference terms corresponding to the Gibbs energies of sodium oxide, sodium peroxide, pure sodium, and pure oxygen, respectively. The Gibbs energy of the liquid phase also contains a configurational entropy term related to mixing of the species on the second sublattice. Finally, excess terms are expressed with the interaction parameters $L^i_{(Na^+)_P(O^{2-},Va^{Q-})_Q}$, $L^0_{(Na^+)_P(O^{2-},Na_2O_2)_Q}$, and $L^i_{(Na^+)_P(Na_2O_2,O)_Q}$, which describe the liquid phase in the Na-Na_2O, Na_2O-Na_2O_2, and Na_2O_2-O composition ranges, respectively, $i = 0,1,2$ corresponding to the order of the interaction parameter.

2.3.4. Gas phase

The gas phase is described by an ideal mixture of (Na, Na_2, Na_2O, O, O_2, O_3) gaseous species. The Gibbs energy is expressed by:

$$G^{\varphi} = \sum_i y_i\cdot{}^{0}G_i^{\varphi} + RT\sum_i y_i lny_i + RTlnP/P^{o} \quad (11)$$

where y_i is the fraction of the species "*i*" in the gas phase. ${}^{o}G_i^{\varphi}$ represents the standard Gibbs energy of the gaseous species "*i*". P^{o} is the standard pressure. The gibbs energy functions were taken from the SGTE database [62].

2.4. Results and discussion

The optimized phase parameters of the liquid phase are given in Table 6 and the calculated temperatures and phase compositions of invariant reactions are listed in Table 7. The phase diagrams calculated with and without the gas phase are shown in Fig. 5 and 6 and represent, respectively, more realistic situations around $x(O) = 1$ (with gas), and around $x(O) = 0$ (without gas, for a closed system where no sodium is allowed to evaporate) (see Table 6).

The phase transitions and melting temperatures of sodium, sodium oxide, sodium peroxide, and sodium superoxide are well described in the present thermodynamic model as shown in Figs. 5 and 6, and Table 7.

The calculated phase diagram reproduces very well the oxygen solubility limit in sodium as determined by Noden [36]. The phase boundaries as determined by Eichelberg [33] are also very close to the calculated curve. The data of Claxton [34,35] deviate to a rather large extent as discussed in Section (2.1). The monotectic equilibrium L1-L2-Na_2O-III is calculated at 1402 K (Fig. 6). The existence of a miscibility gap was never confirmed experimentally, but this would be extremely challenging due to corrosion by the liquid during the experiment [14]. Maupre [27] suggested its occurrence slightly below the melting point of sodium oxide. The author estimated its composition limits on the Na-rich side as 4.7 at% O by extrapolation of the solubility line of Noden, and close to 33.3 at% O on the Na_2O-rich side. Maupre [27] furthermore suggested an eutectic equilibrium β-Na-L1-Na_2O-I at a composition of $6.7\cdot10^{-5}$ at% O by extrapolation of the equation of Noden. The present model reproduces these suggested features.

The eutectic equilibrium Na_2O-I + Na_2O_2-II = liquid at 843 K was never observed experimentally. Its existence was suggested by Wriedt [14] based on the data of Bunzel [29] and Tallman and Margrave [28]. This equilibrium is considered in the present model. The DSC results reported herein make a strong case for the existence of this eutectic equilibrium and are in good agreement with the predicted temperature as shown in Figs. 5 and 6.

Finally the DSC results seem to argue for the existence of a phase transition in Na_2O around 1023 K as observed by Bouaziz et al. [25]. The grey points recorded herein by DSC and depicted on the phase diagrams (see Figs. 5 and 6) are puzzling, however. We would be tempted to assign them to the liquidus equilibria. But this does not fit with the calculated phase diagram, which follows the suggestions of Wriedt [14]. The latter points are at the same level as the sodium oxide first transition temperature, suggesting an incomplete reaction between sodium peroxide and sodium metal in the container, and therefore inducing an error on the composition plotted on these figures. The corresponding measurements can hence unfortunately not be used for the optimization of the liquidus line in the Na_2O-Na_2O_2 composition range.

Table 6
Summary of thermodynamic data for pure elements and oxides selected in the present work. *SER* refers to the phase of the element stable at 298.15 K. The optimized coefficients are marked in bold.

Phase	Gibbs energy (J/mol)	Ref.
Liquid	${}^{o}G_{(Na^{+}:Va^{Q-})} - {}^{o}H_{Na}^{SER} = G_{Na}^{liq}$	[39,41]
$(Na^{+},U^{4+})_P(O^{2-},Na_2O_2,Va^{Q-},O)_Q$	${}^{o}G_{(Na^{+}:O^{2-})} - {}^{o}H_{O}^{SER} - 2{}^{o}H_{Na}^{SER} = G_{Na2O}^{liq}$	[24]
	${}^{o}G_{Na2O2} - 2{}^{o}H_{O}^{SER} - 2{}^{o}H_{Na}^{SER} = G_{Na2O2}^{liq}$	[39]
	$L^{0}(Na^{+})_P(O^{2-},Va^{Q-})_Q$ = **27500+26.3T**	This work
	$L^{1}(Na^{+})_P(O^{2-},Va^{Q-})_Q$ = **32000**	This work
	$L^{0}(Na^{+})_P(O^{2-},Na_2O_2)_Q$ = **−21500**	This work
	$L^{0}(Na^{+})_P(Na_2O_2,O)_Q$ = **1250**	This work
	$L^{1}(Na^{+})_P(Na_2O_2,O)_Q$ = **−11000**	This work
	${}^{o}G_{(U^{4+}:Va^{Q-})} - {}^{o}H_{U}^{SER} = G_{U}^{liq}$	[40]
	${}^{o}G_{(U^{4+}:O^{2-})} - 4{}^{o}H_{U}^{SER} - 2{}^{o}H_{O}^{SER} = 2G_{UO2}^{liq}$	[13]
	$L^{0}(U^{4+})_P(O^{2-},Va^{Q-})_Q$ = 1773475.9-516T	[13]
	$L^{1}(U^{4+})_P(O^{2-},Va^{Q-})_Q$ = 46774.9−120.37888T	[13]
	$L^{2}(U^{4+})_P(O^{2-},Va^{Q-})_Q$ = −500000	[13]
	$L^{0}(U^{4+})_P(O^{2-},O)_Q$ = −370000	[13]
	${}^{o}G_{O}$-${}^{o}H_{O}^{SER} = G_{O}^{SER} - 2648.9 + 31.44T$	[40]
	$L^{0}(Na^{+},U^{4+})_P(Va^{Q-})_Q$ = **100000**	This work
α-U	${}^{o}G_{U}^{\alpha} - {}^{o}H_{U}^{SER} = G_{U}^{SER}$	[40]
β-U	${}^{o}G_{U}^{\alpha} - {}^{o}H_{U}^{SER} = G_{U}^{tet}$	[40]
bcc-phase	${}^{o}G_{(U^{4+}:Va^{Q-})} - {}^{o}H_{U}^{SER} = G_{U}^{bcc}$	[40]
$(Na^{+},U^{4+}:O,Va^{Q-})$	${}^{o}G_{(U^{4+}:O)} - {}^{o}H_{U}^{SER} - {}^{o}H_{O}^{SER} = G_{U}^{bcc} + G_{O}^{SER}$ +100000	[13]
	${}^{o}G_{(Na^{+}:Va^{Q-})} - {}^{o}H_{Na}^{SER} = G_{Na}^{SER}$	[40]
	$L^{0}(Na^{+},U^{4+})(Va^{Q-})$ = **100000**	This work
Gas	${}^{o}G_{Na}^{gas} - {}^{o}H_{Na}^{SER} = G_{Na}^{G}$+RTln($10^{-5}$P)	[62]
$(Na,Na_2,U,UO,UO_2,UO_3,O,O_2,O_3)$	${}^{o}G_{Na_2}^{gas} - 2{}^{o}H_{Na}^{SER} = G_{Na2}^{G}$+RTln($10^{-5}$P)	[62]
	${}^{o}G_{U}^{gas} - {}^{o}H_{U}^{SER} = G_{U}^{G}$+RTln($10^{-5}$P)	[63]
	${}^{o}G_{UO}^{gas} - {}^{o}H_{UO}^{SER} - {}^{o}H_{O}^{SER} = G_{UO}^{G}$+RTln($10^{-5}$P)	[64]
	${}^{o}G_{UO_2}^{gas} - {}^{o}H_{U}^{SER} - 2{}^{o}H_{O}^{SER} = G_{UO_2}^{G}$+RTln($10^{-5}$P)	[64]
	${}^{o}G_{UO_3}^{gas} - {}^{o}H_{U}^{SER} - 3{}^{o}H_{O}^{SER} = G_{UO_3}^{G}$+RTln($10^{-5}$P)	[64]
	${}^{o}G_{O}^{gas} - {}^{o}H_{O}^{SER} = G_{O}^{G}$+RTln($10^{-5}$P)	[62]
	${}^{o}G_{O2}^{gas} - 2{}^{o}H_{O}^{SER} = G_{O2}^{G}$+RTln($10^{-5}$P)	[62]
	${}^{o}G_{O3}^{gas} - 3{}^{o}H_{O}^{SER} = G_{O3}^{G}$+RTln($10^{-5}$P)	[62]
$NaUO_3$	${}^{o}G_{(NaUO_3)} - {}^{o}H_{Na}^{SER} - {}^{o}H_{U}^{SER} - 3{}^{o}H_{O}^{SER} = G_{NaUO3}$	This work
Na_3UO_4	${}^{o}G_{(Na3UO4)} - 3{}^{o}H_{Na}^{SER} - {}^{o}H_{U}^{SER} - 4{}^{o}H_{O}^{SER} = G_{Na3UO4}$	This work
α-Na_2UO_4	${}^{o}G_{(\alpha-Na2UO4)} - 2{}^{o}H_{Na}^{SER} - {}^{o}H_{U}^{SER} - 4{}^{o}H_{O}^{SER} = G_{\alpha-Na2UO4}$	This work
β-Na_2UO_4	${}^{o}G_{(\beta-Na2UO4)} - 2{}^{o}H_{Na}^{SER} - {}^{o}H_{U}^{SER} - 4{}^{o}H_{O}^{SER} = G_{\beta-Na2UO4}$	This work
Na_4UO_5	${}^{o}G_{(Na4UO5)} - 4{}^{o}H_{Na}^{SER} - {}^{o}H_{U}^{SER} - 5{}^{o}H_{O}^{SER} = G_{Na4UO5}$	This work
α-$Na_2U_2O_7$	${}^{o}G_{(\alpha-Na2U2O7)} - 2{}^{o}H_{Na}^{SER} - 2{}^{o}H_{U}^{SER} - 7{}^{o}H_{O}^{SER} = G_{\alpha-Na2U2O7}$	This work
β-$Na_2U_2O_7$	${}^{o}G_{(\beta-Na2U2O7)} - 2{}^{o}H_{Na}^{SER} - 2{}^{o}H_{U}^{SER} - 7{}^{o}H_{O}^{SER} = G_{\beta-Na2U2O7}$	This work
G_{O}^{SER}	$= 1/2{}^{o}G_{O2}^{G}$	[40]
G_{Na}^{SER}	$= -11989.434 + 260.548732T - 51.0393608Tln(T) + 7.2306633\cdot10^{-2}T^{2} - 4.3638283\cdot10^{-5}T^{3} + 132154T^{-1}$ (298.15K<T<370.87 K)	[40]
	$=-11009.884 + 199.619999T - 38.1198801Tln(T) + 9.745854\cdot10^{-3}T^{2} - 1.70664\cdot10^{-6}T^{3} + 34342T^{-1} + 1.65071\cdot10^{23}T^{-9}$(T>370.87 K)	[40]
G_{Na}^{liq}	$=G_{Na}^{SER} + 2581.02 - 6.95218T$ (298.15<T<370.87 K)	[40]
	$=-8400.44952 + 192.58736928T - 38.11988Tln(T) + 9.745855\cdot10^{-3}T^{2} - 1.70664\cdot10^{-6}T^{3} + 34342.48T^{-1}$ (T>370.87K)	[40]
G_{Na2O}^{liq}	$=-401097.3 + 608.877T - 104.6Tln(T)$	[24]
G_{Na2O2}^{liq}	$=-530252.15 + 678.6366T - 117.15Tln(T)$	[39]
G_{U}^{SER}	$=-8407.734 + 130.955151T - 26.9182Tln(T) + 1.25156\cdot10^{-3}T^{2} - 4.42605\cdot10^{-6}T^{3} + 38568T^{-1}$ (298.15K<T<955K)	[40]
	$=-22521.8 + 292.121093T - 48.66Tln(T)$ (T>955K)	
G_{U}^{tet}	$=-5156.136 + 106.976316T - 22.841Tln(T) - 1.084475\cdot10^{-2}T^{2} + 2.7889\cdot10^{-8}T^{3} + 81944T^{-1}$ (298.15K<T<941.5K)	[40]
	$=-14327.309 + 244.16802T - 42.9278Tln(T)$ (T>941.5K)	
G_{U}^{bcc}	$=-752.767 + 131.5381T - 27.5152Tln(T) - 8.35595\cdot10^{-3}T^{2} + 9.67907\cdot10^{-7}T^{3} + 204611T^{-1}$ (298.15K<T<1049K)	[40]
	$=-4698.365 + 202.685635T - 38.2836Tln(T)$ (T>1049K)	
G_{U}^{liq}	$=+3947.766 + 120.631251T - 26.9182Tln(T) + 1.25156\cdot10^{-3}T^{2} - 4.42605\cdot10^{-6}T^{3} + 38568T^{-1}$ (T<955K)	[40]
G_{U}^{liq}	$=-10166.3 + 281.797193T - 48.66Tln(T)$ (T>955K)	[40]
G_{UO2}^{liq}	$= G_{UO2} + 79775 - 25.0114T - 2.62269566\cdot10^{-21}T^{7}$ (298.15K<T<2600K)	[13]
	$=-1590418 + 3618.8T - 480Tln(T) + 0.07T^{2} - 10^{-6}T^{3}$ (T>2600K)	[13]
G_{UO2}	$= -1118940.2 + 554.00559T - 93.268Tln(T) + 1.01704254\cdot10^{-2}T^{2} - 2.03335671\cdot10^{-6}T^{3} + 1091073.7T^{-1}$	[13]
G_{NaUO3}	$=-1536709.4 + 708.03476T - 123.187Tln(T)-0.00318T^{2} + 713705T^{-1} - 2.08206667\cdot10^{-7}T^{3}$	This work
G_{Na3UO4}	$=-2093081.6 + 1161.25595T - 200.388Tln(T)-0.00341T^{2} + 1339645T^{-1} - 8.73891667\cdot10^{-7}T^{3}$	This work

Table 6 (*continued*)

Phase	Gibbs energy (J/mol)	Ref.
$G_{\alpha-Na2UO4}$	$=-1960565.4 + 986.57642T - 170.071T\ln(T) - 0.006605T^2 + 1201780T^{-1} - 1.88046667\cdot10^{-7}T^3$	This work
$G_{\beta-Na2UO4}$	$= G_{\alpha-Na2UO4} + 25400 - 21.29086T$	This work
G_{Na4UO5}	$=-2538960.0 + 1404.35175T - 243.746T\ln(T) - 0.008075T^2 + 1270595T^{-1} - 8.7079\cdot10^{-7}T^3$	This work
$G_{\alpha-Na2U2O7}$	$=-3295702.9 + 1512.22589T - 262.781T\ln(T) - 0.01206T^2 + 1860870T^{-1} + 1.12823667\cdot10^{-9}T^3$	This work
$G_{\beta-Na2U2O7}$	$= G_{\alpha-Na2U2O7} + 2800 - 4.66667T$	This work

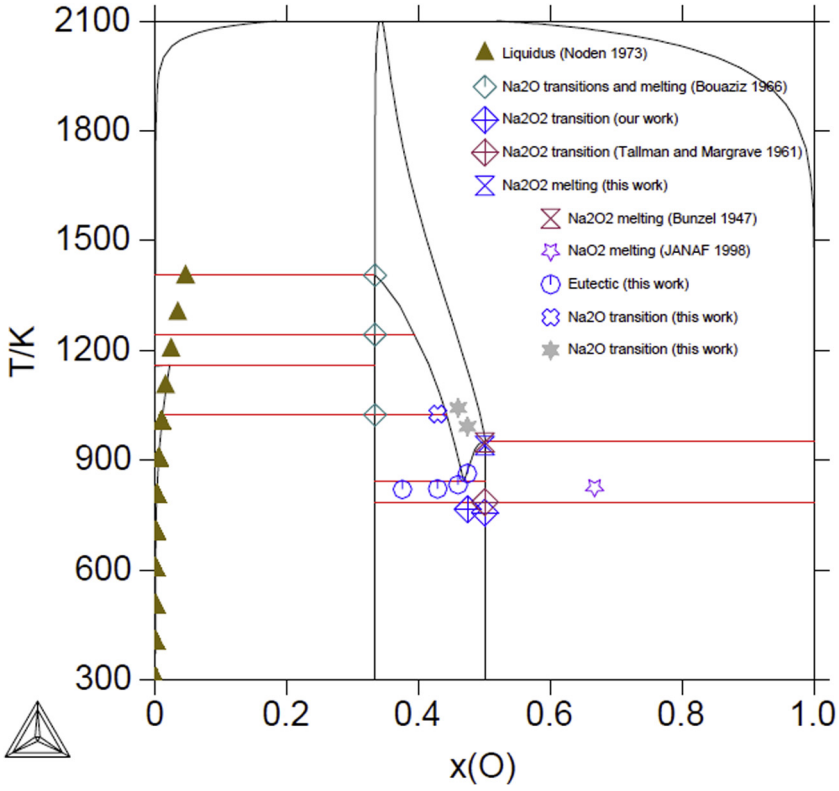

Fig. 5. Calculated Na-O phase diagram at 1 bar considering the gas phase, and comparison with the experimental data.

3. Thermodynamic assessment of the Na-U-O system

3.1. Review of literature data

3.1.1. Phase diagram data

The known compounds in the Na-U-O phase diagram are numerous (Na_2UO_4, Na_4UO_5, $Na_2U_2O_7$, $NaUO_3$, Na_3UO_4) and their structural properties are now well established. A summary of the crystal symmetries and cell parameters for these phases is provided in Table 10. Further details on the local coordination geometries for each structure can be found in other publications [65–69].

Pentavalent $NaUO_3$ has a perovskite structure, in space group *Pbnm* [70]. $Na_2U_2O_7$ has three polymorphs. The stable phase at room temperature, α-$Na_2U_2O_7$, has monoclinic symmetry in space group $P2_1/a$ [67], and transforms between 573 and 623 K to β-$Na_2U_2O_7$, which is monoclinic in space group $C2/m$ [67,68]. The second transition to the high-temperature γ rhombohedral structure occurs between 1223 and 1323 K [68]. Hexavalent Na_2UO_4 shows two polymorphs with a phase transition measured at 1193 K [71]. The α and β phases are orthorhombic in space group *Pbam* and *Pbca*, respectively [71]. Na_4UO_5 has tetragonal symmetry, in space group $I4/m$ [72]. In addition, Smith et al. reported the existence of a low temperature metastable phase for this composition, i.e., *m*-Na_4UO_5, with disordered NaCl cubic type of structure [66]. The uranium valency in those compounds was moreover investigated using X-ray Absorption Near Edge Spectroscopy (XANES) at the U-L_3 edge for $NaUO_3$, α-$Na_2U_2O_7$, Na_4UO_5 [65], α-Na_2UO_4 [73], and at the U-M_4 edge for *m*-Na_4UO_5 [66], which confirmed the chemical compositions established by X-ray diffraction.

Finally, the case of the trisodium uranate Na_3UO_4 is particularly complex and requires a more detailed description. Three polymorphs were reported in the literature, but their structures were the subject of controversy until recently. Scholder and Gläser [74] first reported in 1964 a disordered NaCl type of structure, obtained at low temperatures ($T < 973$ K), with cell parameter 4.77 Å. The investigations of Smith et al. showed that the latter phase probably corresponded to a metastable *m* phase and questioned the assigned chemical composition [66]. Bartram and Fryxell obtained at temperatures ranging from 973 to 1273 K a stable ordered α phase with many additional reflections, which they assigned to cubic symmetry with a doubled cell parameter (9.54 Å) and the chemical composition $Na_{11}U_5O_{16}$ [75,76]. The latter assignment was ruled out by Smith et al., however, who found the α form of trisodium uranate to be monoclinic, in space group

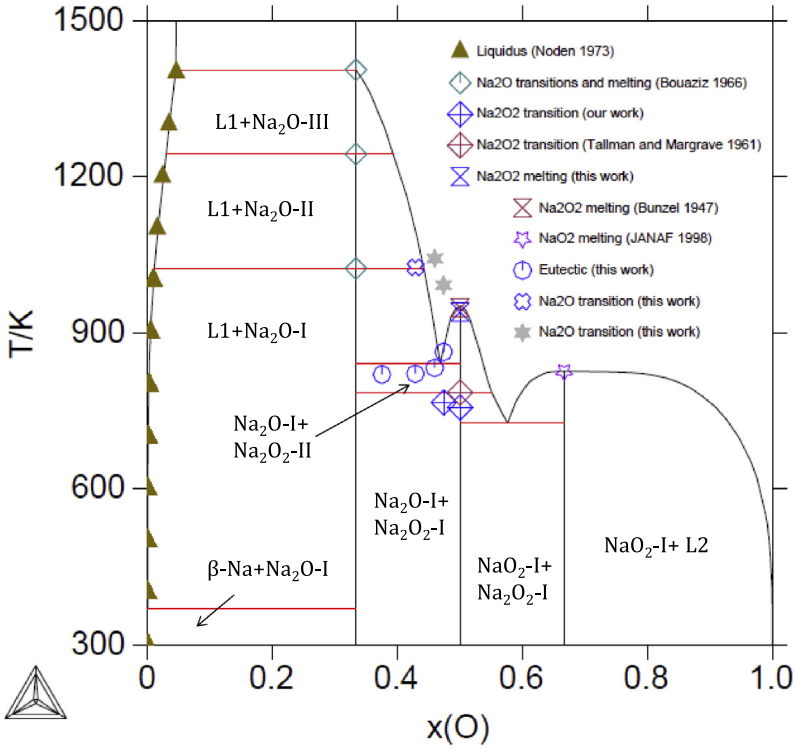

Fig. 6. Calculated Na-O phase diagram at 1 bar excluding the gas phase, and comparison with the experimental data.

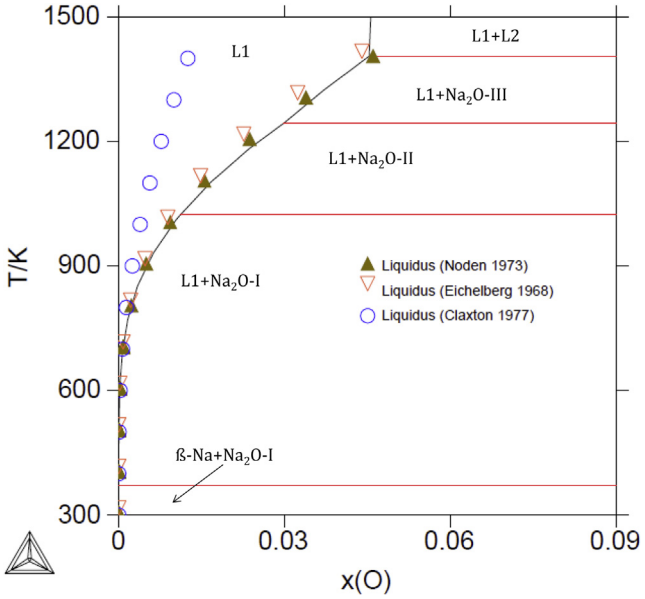

Fig. 7. Calculated Na-O phase diagram at 1 bar excluding the gas phase, and comparison with the experimental data for the oxygen solubility in sodium.

$P2/c$ [66]. In addition, the authors showed on the basis of X-ray, neutron diffraction, XANES, and ^{23}Na MAS NMR data that the α phase could accommodate some cationic disorder on the uranium site with the incorporation of up to 16(2)% excess sodium, corresponding to the mixed valence state composition $Na_3(U_{1-x}Na_x)O_4$ ($0.14 < x < 0.18$). The $Na_3(U_{1-x}Na_x)O_4$ formula with $x = 0$ and $x = 0.2$ corresponds to the Na_3UO_4 and Na_4UO_5 stoichiometric compositions, respectively. The $\alpha - Na_{3.16(2)}U_{0.84(2)}O_4$ compound synthesized by [66] is hence found on the pseudobinary section between $Na_3U^{V}O_4$ and $Na_4U^{VI}O_5$ end-members, rather close to the latter composition, as shown in the equilibrium phase diagram in Fig. 12, corresponding to an uranium mean valence state of 5.69(6) [66]. Finally the semi-ordered high temperature β modification of Na_3UO_4 is cubic, in space group $Fd\bar{3}m$ as described in the work of [66,77].

Although the structural properties of the sodium uranates are now well-known, the phase relationships in the Na-U-O phase diagram have not been investigated systematically. A sketch of the isotherm at 1273 K (shown in Fig. 8) has been reported based on the various crystallographic and thermodynamic studies [9,78], but the phase boundaries, tri-phasic domains and evolution with temperature of the equilibrium phases have not been determined.

3.1.2. Thermodynamic functions

The thermodynamic data available for the sodium uranates are quite complete as shown in Table 8 [43,79]. Enthalpies of formation at 298.15 K were determined using solution calorimetry, while entropies and heat capacities were derived using adiabatic and thermal relaxation calorimetry.

The high temperature enthalpy increments of $NaUO_3$ [81], α- and β-Na_2UO_4 [71,82], α- Xand β-$Na_2U_2O_7$ [81] were measured using drop calorimetry, yielding the fitted heat capacity functions listed in Table 9. The transition enthalpy for Na_2UO_4 was reported as $\Delta_{tr}H^{\circ}_{m}(Na_2UO_4, cr, 1193K) = 25.4\ kJ{\cdot}mol^{-1}$, based on the differential thermal analysis (DTA) measurements by Cordfunke and IJdo [71] and enthalpy increment measurements by Fredrickson and O'Hare using drop calorimetry [82]. The transition was found reversible but very slow near the transition temperature [71]. The enthalpy increment data for $Na_2U_2O_7$ cover only the temperature ranges 390–540 K (α form) and 681–926 K (β form), respec-

Table 7
Invariant reactions in the Na-O system (L = liquid).

Invariant reaction	Transition type	T/K	Phases composition x(O)	Reference
β-Na = L1	melting	370.98	0	Present work
		370.98 ± 0.02	0	[24]
Na_2O-I = Na_2O-II	polymorphic	1020.3	0.333	Present work
		1023.2	0.333	[24]
Na_2O-II = Na_2O-III	polymorphic	1241	0.333	Present work
		1243.2	0.333	[24]
Na_2O-III = L2	melting	1403	0.333	Present work
		1405.2	0.333	[24]
Na_2O_2-I = Na_2O_2-II	polymorphic	782	0.5	Present work
		785 ± 1	0.5	[24]
Na_2O_2-II = L2	melting	948	0.5	Present work
		948	0.5	[24]
NaO_2-I = L2	melting	826	0.667	Present work
		825 ± 10	0.667	[24]
Na_2O-III + L1 = L2	monotectic	1402	Na_2O(0.333);L1(0.047);L2(~0.333)	Present work
		1403	Na_2O(0.333);L1(0.047);L1(<0.333)	[14]
β-Na + Na_2O-I = L1	eutectic	370.98	β-Na(0); Na_2O(0.333);L1(6.4×10^{-7})	Present work
		371	β-Na(0); Na_2O(0.333);L1($6.7 \cdot 10^{-5}$);	[14]
Na_2O-I + Na_2O_2-II = L2	eutectic	843	$Na_2O_{(I)}$(0.333); L2(0.47);$Na_2O_{2\ II}$(50)	Present work
		843	Na_2O_I(0.333); L2(0.44);$Na_2O_{2(II)}$(<50);	[29,18]

tively [81]. The $\alpha \rightarrow \beta$ transition temperature and associated transition enthalpy are not known, but should be very small $(\Delta_{tr}H^{o}_{m}(600K) - \Delta_{tr}H^{o}_{m}(298.15K) \sim 1.6\ kJ \cdot mol^{-1}$ at 600 K [68]). The kinetics of the transition were also found to be particularly slow [68,81]. The values for the enthalpy increments of β-$Na_2U_2O_7$ [81] could in fact not be fitted reliably as the thermodynamic parameters at 298.15 K and at the transition temperature were not determined [80]. No thermodynamic functions were reported for the γ form. Complementary calorimetric studies covering temperatures above 926 K are required for a proper description of this phase. In the present thermodynamic model, we have considered the α- and β-$Na_2U_2O_7$ phases only, and used an extrapolation of the heat capacity function of $Na_2U_2O_7$ in the temperature range where the γ form is stable. This model can be re-visited in the future once the Gibbs energy functions of β and γ-$Na_2U_2O_7$ have been determined experimentally. Finally, the heat capacity at high temperatures of Na_4UO_5 was not measured to this date.

The case of trisodium uranate Na_3UO_4 requires particular attention as its crystal structure was the subject of controversy as discussed in Section (3.1.1) [66]. A single batch of Na_3UO_4 material was prepared by O'Hare et al. [84] in 1972, which was used to determine its enthalpy of formation [84], heat capacity and entropy at 298.15 K [83], and enthalpy increments in the temperature range 523–1212 K [85] using solution, adiabatic, and drop calorimetry, respectively.

The sample was prepared by heating a mixture of sodium oxide of composition $Na_2O_{1.05}$, with uranium oxide of composition $UO_{2.14}$, and excess sodium in proportions corresponding to the following reaction [84]:

$$UO_{2.14} + 1.77Na_2O_{1.05} = Na_3UO_4 + 0.54Na \quad (12)$$

The authors reported the X-ray diffraction pattern appeared "fairly complicated", with the "principal lines [...] indexed as *f.c.c.* pattern with a lattice parameter of 4.77 Å", but corresponding "essentially [to] that reported by Bartram and Fryxell" [84], and to which the wrong composition $Na_{11}U_5O_{16}$ was initially attributed [76]. From this description, we deduce that the thermodynamic measurements were carried out on the α form of the trisodium uranate [66]. It should also be noted that the compound prepared was not completely pure, but contained (2.0 ± 1.8) wt% of uranium dioxide impurity. As for the high temperature β form of the same compound and metastable *m* cubic form, there are no data available. Extending the thermodynamic functions to higher temperatures, and estimating the enthalpy of transition to the β phase would be of particular interest for the safety assessment of the fuel-sodium interaction.

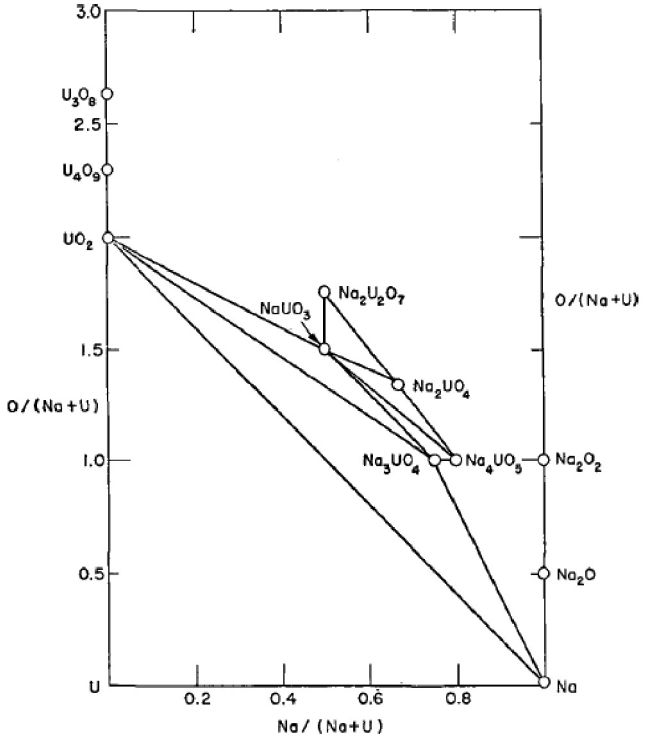

Fig. 8. Ternary Na-U-O phase diagram at 1273 K as reported by Blackburn et al. [9], reproduced with permission by the IAEA.

3.1.3. Vaporization studies

Vapour pressure studies in the Na-U-O system were reported using Knudsen effusing mass loss (KEML), Knudsen effusion mass spectrometry (KEMS) and the transpiration technique [86–88,68]. A more detailed description of these investigations can be found in [68]. The sodium pressure measured over the six ternary phase fields Na-UO_2-Na_3UO_4, UO_2-$NaUO_3$-Na_3UO_4, $NaUO_3$-Na_4UO_5-Na_3UO_4, $NaUO_3$-Na_2UO_4-Na_4UO_5, $NaUO_3$-Na_2UO_4-$Na_2U_2O_7$, and

Table 8
Thermodynamic data for the Na-U-O ternary phases measured experimentally* [80,43], calculated in this work using DFT, and optimized in the CALPHAD model.

Compound	$\Delta_f H^o_m$ (298.15 K)/ kJ·mol^{-1}	S^o_m (298.15 K)/ J·K^{-1}·mol^{-1}	$C^o_{p,m}$ (298.15 K)/ J·K^{-1}·mol^{-1}	$\Delta_f G^o_m$ (298.15 K)/ kJ·mol^{-1}	Reference
α-Na_2UO_4	−1897.7 ± 3.5	166.0 ± 0.5	146.7 ± 0.5	−1779.3 ± 3.5	[43]
	−1858.1	*191.5*	*150.2*	*−1747.5*	DFT-this work
	−1901.2	**170.0**	**147.1**	**−1784.0**	CALPHAD-this work
β-Na_2UO_4	−1884.6 ± 3.6	–	–	–	[43]
	−1852.2	*181.8*	*150.1*	*−1738.9*	DFT-this work
Na_4UO_5	−2457.0 ± 2.2	247.5 ± 6.2	220.6 ± 6.7	−2301.7 ± 2.9	[43,79]
	−2388.3	*252.4*	*216.9*	*−2234.7*	DFT-this work
	−2457.0	**247.5**	**220.4**	**−2301.7**	CALPHAD-this work
α-$Na_2U_2O_7$	−3203.8 ± 4.0	275.9 ± 1	227.3 ± 1	−3011.5 ± 4.0	[43]
	−3130.5	*331.3*	*229.5*	*−3130.5*	DFT-this work
	−3203.8	**275.9**	**228.1**	**−3011.5**	CALPHAD-this work
β-$Na_2U_2O_7$	*−3130.8*	*311.1*	*230.6*	*−2949.1*	DFT-this work
$NaUO_3$	−1494.9 ± 10	132.8 ± 0.40	108.87 ± 0.40	−1412.5 ± 10	[43]
	−1494.6	*134.3*	*109.8*	*−1412.7*	DFT-this work
	−1494.9	**127.0**	**109.1**	**−1410.8**	CALPHAD-this work
α-Na_3UO_4	−2024.0 ± 8.0	198.2 ± 0.4	173.0 ± 0.4	−1899.9 ± 8	[43]
	−2014.7	*206.3*	*175.7*	*−1893.2*	DFT-this work
	−2024.0	**198.2**	**172.8**	**−1899.9**	CALPHAD-this work

*The reported uncertainties correspond to standard uncertainties.

Table 9
Summary of the heat capacity functions for the sodium uranates derived from drop calorimetry enthalpy increment data.

Compound	$C_{p,m} = A + B{\cdot}T + E{\cdot}T^{-2}$/(J·K^{-1}·mol^{-1})			T/K	Reference
	A	B	E		
$NaUO_3$	115.49	$19.167{\cdot}10^{-3}$	$-10.966{\cdot}10^{5}$	298.15-931	[81]
α-Na_3UO_4	188.901	$25.1788{\cdot}10^{-3}$	$-20.801{\cdot}10^{5}$	298.15–1212	[83]
α-Na_2UO_4	162.5688	$25.8588{\cdot}10^{-3}$	$-21.00428{\cdot}10^{5}$	298.15–1165	[71,82]
β-Na_2UO_4	70.4254	$119.4756{\cdot}10^{-3}$	$+102.057{\cdot}10^{5}$	298.15–1273	[71,82]
α-$Na_2U_2O_7$	262.83	$14.653{\cdot}10^{-3}$	$-35.490{\cdot}10^{5}$	298.15–540	[81]
β-$Na_2U_2O_7$	280.57			681–786	[81]

$NaUO_3$-$Na_2U_2O_7$-UO_2 are shown in Fig. 9 and compared to the data derived from the model in Figs. 13–15.

3.2. Ab-initio calculations combined with a quasi-harmonic model

3.2.1. Description of the method

The method used to calculate the thermodynamic functions of the sodium uranate phases using ab initio calculations at 0 K and a quasi-harmonic statistical thermodynamic model to derive the temperature dependency of the thermodynamic properties is briefly described hereafter. A more exhaustive description can be found in [89].

This method requires only information on the crystal symmetry and space group, lattice parameters, and atomic position coordinates as starting point. The following three approximations are used to derive the free energy of a crystal containing N cells with n atoms per cell:

(i) The adiabatic approximation to calculate the cohesive energy of the crystal $E_{cohesive}$ versus static pressure at zero kelvin, and correspondingly versus the equilibrium volume V.
(ii) The harmonic approximation to calculate the $3n$ vibration frequencies $v_j(\vec{q})$ $(j = 1, 3n)$ for N values of wave vector $\vec{q}$ in the first Brillouin zone. These $3n$ frequencies dispersion branches are divided into three acoustic branches and $(3n - 3)$ optical branches. Satisfactory accuracy is obtained by computing optical vibration frequencies at the Γ point only $(\vec{q} = 0)$ providing the unit cell is large enough. For $\vec{q} \neq 0$ we use the Debye model to determine the acoustic vibration frequencies and the Einstein model for the optical vibration frequencies. From $E_{cohesive}(V)$ and the frequencies $v_j(\vec{q} = 0)$ $(j = 1, 3n)$ it is possible to construct the partition function of the crystal and deduce its free energy at temperature T by the statistical thermodynamic laws:

$$F = -E_{cohesive}(V) + Nk_BT\left[\frac{9}{8}x_D + 3ln(1-e^{-x_D}) - D(x_D) + \sum_{j=1}^{3n-3}\left(\frac{x_j}{2} + ln(1-e^{-x_j})\right)\right] \quad (13)$$

where $x_j = hv_j(0)/k_BT$. $D(x_D)$ is the Debye function with $x_D = \theta_D/T$ where θ_D is the Debye temperature. k_B and h are the Boltzmann and Planck constants, respectively. For an ideal isotropic crystal [89] θ_D is given by:

$$\theta_D = \frac{h}{k_B}\left(\frac{9}{4\pi V}\right)^{1/3}\left(3\frac{B}{\rho}\right)^{1/2}\left(\frac{1-\sigma^0}{1+\sigma^0}\right)^{1/2}\left[1+2\left(\frac{2-2\sigma^0}{1-2\sigma^0}\right)^{3/2}\right]^{-1/3} \quad (14)$$

where B is the bulk modulus, ρ is the density, and σ^0 is the Poisson ratio (close to 0.33).

(iii) To account for the thermal expansion while maintaining the simplicity of the harmonic model, the quasi-harmonic approximation is used assuming that the vibration frequencies change with the volume of the unit cell:

Table 10
Parameters and results of the ab initio calculations using the CASTEP Code [90]. DFT lattice parameters (nm) and equilibrium volume of unit cell (nm^3) at zero temperature and pressure, in italics, are compared to the reference experimental data. Note that all volumes calculated with DFT are systematically larger than the experimental data. This well-known behaviour is related to the generalized gradient approximation form of the exchange/correlation energies. Experimental lattice parameters were obtained at atmospheric pressure (0.10 ± 0.01) MPa. ***Vol.*** = volume of the unit cell. RT = (295 ± 2)K.

Phase	Sym.	Z	Space group	*a*/nm Exp. *calc.*	*b*/nm Exp. *calc.*	*c*/nm Exp. *calc.*	*β* /° Exp. *calc.*	Vol./nm^3 Exp. *calc.*	T/K Exp. *calc.*	DFT band gap (eV)	Ref.
$NaUO_3$	Ortho.	4	*Pbnm* (62)	0.57739[a]	0.59051[a]	0.82784[a]	90	0.28226[a]	RT		[70]
				0.58321	*0.59742*	*0.83699*	*90*	*0.29187*	0	*1.809*	*DFT*
m-Na_3UO_4	Cubic	1	$Fm\bar{3}m$ (225)	0.477[b]	0.477[b]	0.477[b]	90	0.10853	RT		[74]
α-$Na_{3.16(2)}U_{0.84(2)}O_4$	Mono.	2	*P*2/*c* (14)	0.5892[c]	0.6772[c]	0.5916[c]	110.65[c]	0.22083[c]	RT		[66]
α-Na_3UO_4	*Mono.*	*2*	*P*2/*c* (14)	*0.5937*	*0.6845*	*0.5978*	*110.540*	*0.22730*	0	*1.873*	*DFT*
β-$Na_{3+x}U_{1-x}O_4$	Cubic	8	$Fd\bar{3}m$ (227)	0.9589[c]	0.9589[c]	0.9589[c]	90	0.88191[c]	RT		[66]
β-Na_3UO_4	Cubic	8	$Fd\bar{3}m$ (227)	0.956[d]	0.956[d]	0.956[d]	90	0.8737[d]	RT		[77]
α-Na_2UO_4	Ortho.	2	*Pbam* (55)	0.97623[e]	0.57287[e]	0.34956[e]	90	0.195496[e]	RT		[71]
				1.00103	*0.57628*	*0.35236*	*90*	*0.203352*	0	*2.253*	*DFT*
β-Na_2UO_4	Ortho.	4	*Pbca* (61)	0.58079[f]	0.59753[f]	1.17179[f]	90	0.406650[f]	RT		[71]
				0.58598	*0.60265*	*1.18836*	*90*	*0.419514*	0	*2.489*	*DFT*
m-Na_4UO_5	Cubic	1	$Fm\bar{3}m$ (225)	0.4764[g]	0.4764[g]	0.4764[g]	90	0.10812[g]	RT		[66]
Na_4UO_5	Tetra.	2	*I*4/*m* (87)	0.75172[h]	0.75172[h]	0.46325[h]	90	0.26178[h]	RT		[72]
				0.76950	*0.76950*	*0.46325*	*90*	*0.27542*	0	*2.522*	*DFT*
α-$Na_2U_2O_7$	Mono.	4	$P2_1/a$ (14)	1.27617[i]	0.78384[i]	0.68962[i]	111.285[i]	0.64278[i]	293		[67]
				1.31322	*0.78815*	*0.69292*	*110.994*	*0.66918*	0	*2.169*	DFT
β-$Na_2U_2O_7$	Mono.	4	*C*2/*m* (12)	1.2933[j]	0.7887[j]	0.69086[j]	110.816[j]	0.65880[j]	773		[67]
				1.3125	*0.7881*	*0.69291*	*110.967*	*0.66933*	0	*2.161*	DFT
γ-$Na_2U_2O_7$	Rhombo.	3/2	$R\bar{3}m$ (166)	0.3987[k]	0.3987[k]	1.8491[k]	90	0.25461[k]	1323		[68]

Standard uncertainties *u* are [a]*u*(*a*) = 0.00002 nm, *u*(*b*) = 0.00002 nm, *u*(*c*) = 0.00002 nm, *u*(Vol.) = 0.00001 nm^3.
Standard uncertainties *u* are [b]*u*(*a*) = 0.002 nm, *u*(*b*) = 0.002 nm, *u*(*c*) = 0.002 nm, *u*(Vol.) = 0.0001 nm^3.
Standard uncertainties *u* are [c]*u*(*a*) = 0.0002 nm, *u*(*b*) = 0.0002 nm, *u*(*c*) = 0.0002 nm, *u*(*β*) = 0.02, *u*(Vol.) = 0.00001 nm^3.
Standard uncertainties *u* are [d]*u*(*a*) = 0.004 nm, *u*(*b*) = 0.004 nm, *u*(*c*) = 0.004 nm, *u*(Vol.) = 0.0001 nm^3.
Standard uncertainties *u* are [e]*u*(*a*) = 0.00003 nm, *u*(*b*) = 0.00002 nm, *u*(*c*) = 0.00001 nm, *u*(Vol.) = 0.000011 nm^3.
Standard uncertainties *u* are [f]*u*(*a*) = 0.00003 nm, *u*(*b*) = 0.00003 nm, *u*(*c*) = 0.00006 nm, *u*(Vol.) = 0.000034 nm^3.
Standard uncertainties *u* are [g]*u*(*a*) = 0.0003 nm, *u*(*b*) = 0.0003 nm, *u*(*c*) = 0.0003 nm, *u*(Vol.) = 0.00001 nm^3.
Standard uncertainties *u* are [h]*u*(*a*) = 0.00001 nm, *u*(*b*) = 0.00001 nm, *u*(*c*) = 0.00002 nm, *u*(Vol.) = 0.00001 nm^3.
Standard uncertainties *u* are [i]*u*(*a*) = 0.000014 nm, *u*(*b*) = 0.000010 nm, *u*(*c*) = 0.00009 nm, *u*(*β*) = 0.009 , *u*(Vol.) = 0.00010 nm^3.
Standard uncertainties *u* are [j]*u*(*a*) = 0.0001 nm, *u*(*b*) = 0.0001 nm, *u*(*c*) = 0.00008 nm, *u*(*β*) = 0.010 , *u*(Vol.) = 0.00013 nm^3.
Standard uncertainties *u* are [k]*u*(*a*) = 0.0003 nm, *u*(*b*) = 0.0003 nm, *u*(*c*) = 0.0003 nm, *u*(Vol.) = 0.00001 nm^3.

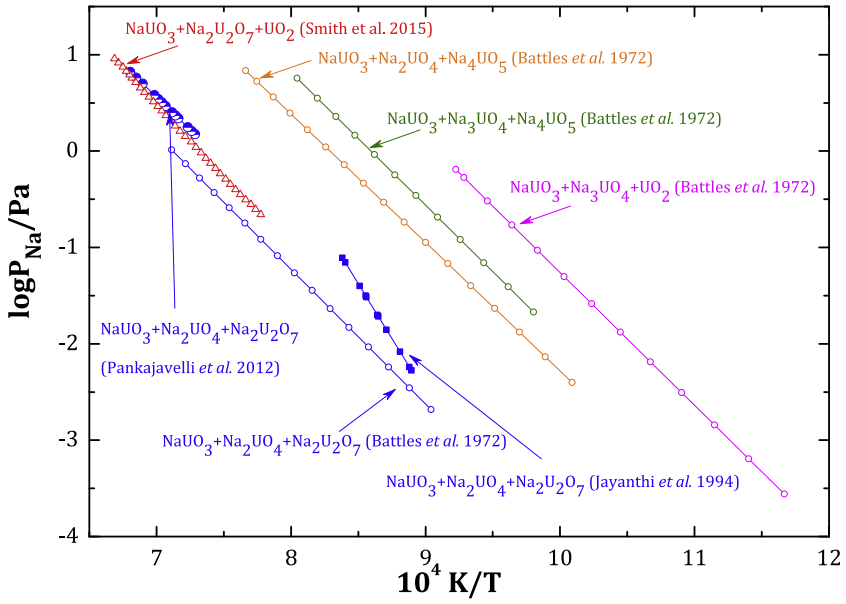

Fig. 9. Sodium partial pressure measured in the ternary phase fields of the Na-U-O phase diagram [86–88,68].

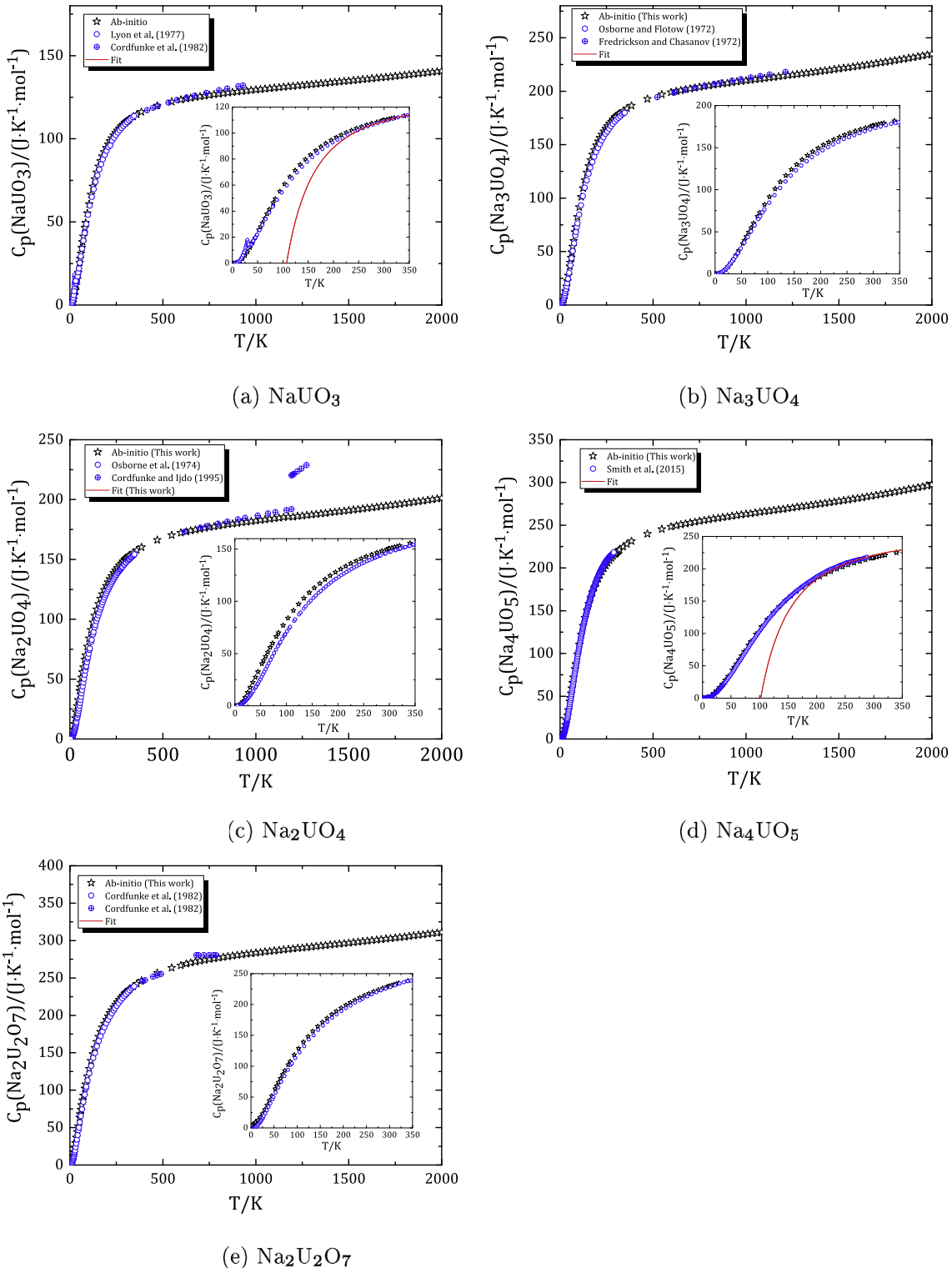

Fig. 10. Calculated heat capacity data using the DFT and quasi-harmonic model (★), and comparison with the experimental heat capacity data reported in the literature (⊗, ◯). The regression laws used for the CALPHAD model and reported in Table 11 are shown as plain red lines.

$$pV = V\frac{dE_{cohesive}(V)}{dV} + Nk_BT\left[\gamma_{acoustic}\left(\frac{9}{8}x_D + 3D(x_D)\right) + \gamma_{optic}\sum_{j=1}^{3n-3}\left(\frac{x_j}{2} + \frac{x_j}{e^{x_j}-1}\right)\right] \quad (15)$$

where $\gamma_{acoustic}$ and γ_{optic} are the Grüneisen coefficients. For an ideal isotropic crystal these Grüneisen coefficients are given by [89]:

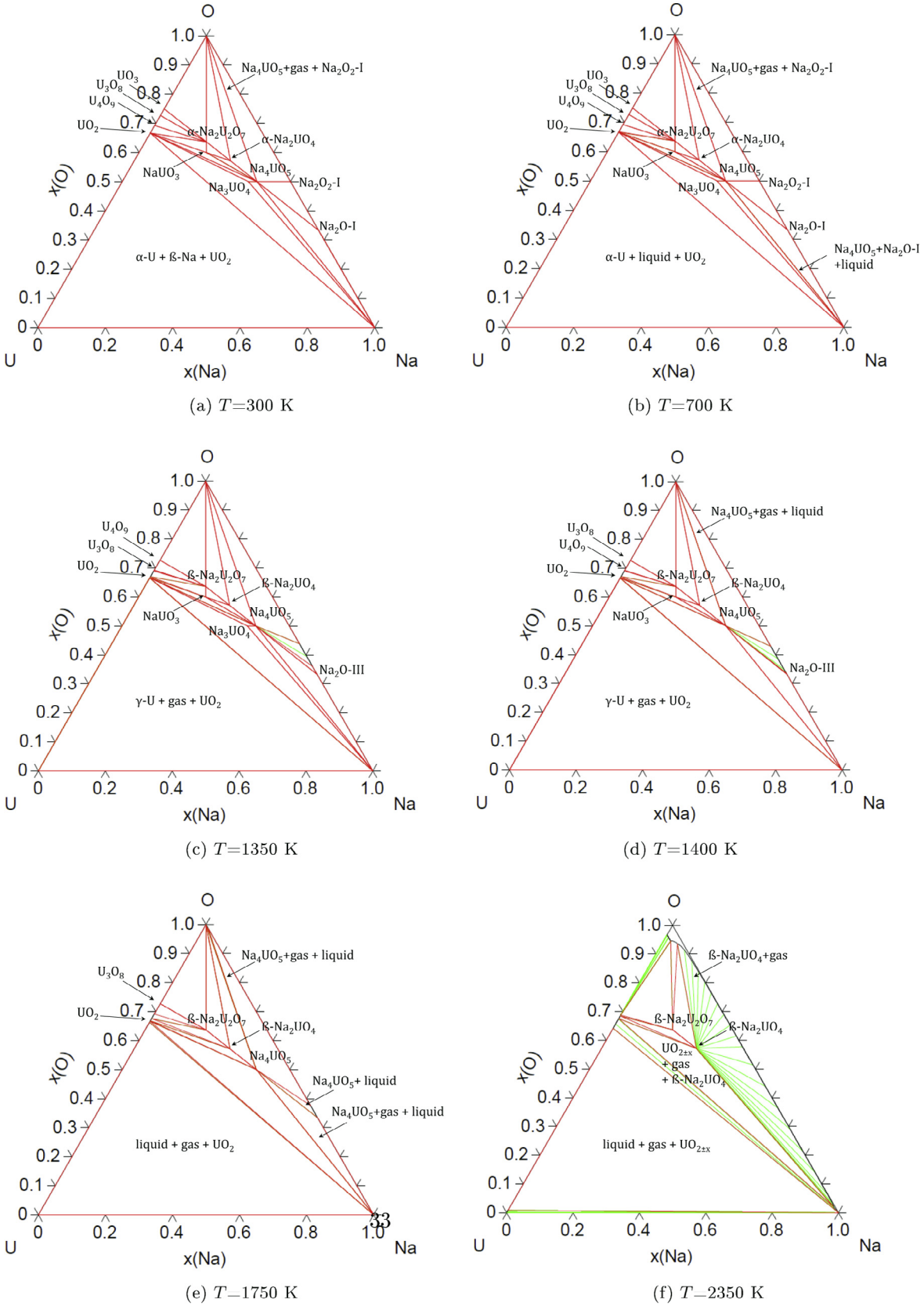

(a) T=300 K (b) T=700 K

(c) T=1350 K (d) T=1400 K

(e) T=1750 K (f) T=2350 K

Fig. 11. Calculated Na-U-O phase diagrams at (T = 300,700,1350,1400,1750,2350 K) and 1 bar

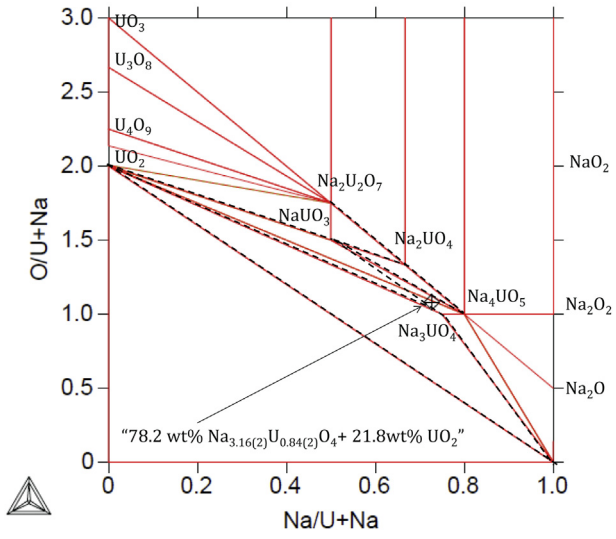

Fig. 12. Calculated Na-U-O phase diagram at 900 K and 1 bar (red line), and comparison with the phase boundaries between the ternary phase fields as suggested by [9] (black dotted line). (For interpretation of the references to colour in this figure legend, the reader is referred to the web version of this article.)

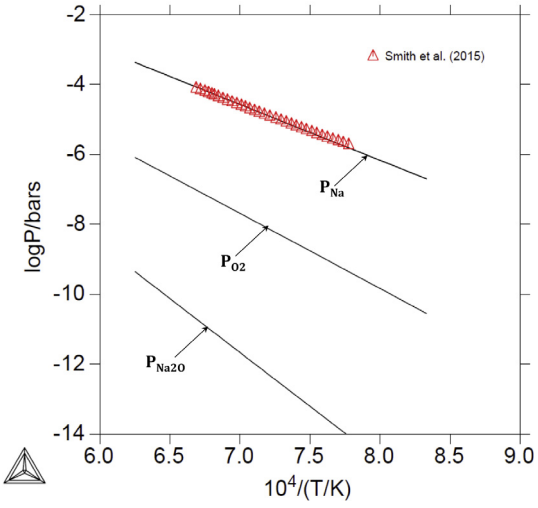

Fig. 13. Sodium and oxygen partial pressures calculated in the ternary phase field $NaUO_3$-$Na_2U_2O_7$-UO_2 and comparison with literature data [68].

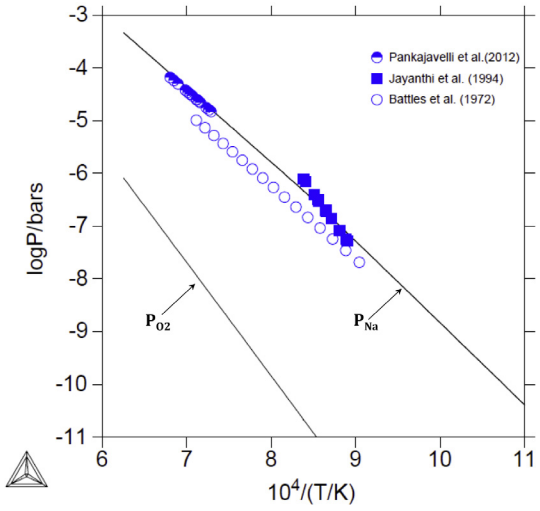

Fig. 14. Sodium and oxygen partial pressures calculated in the ternary phase field $NaUO_3$-Na_2UO_4-$Na_2U_2O_7$ and comparison with literature data [86–88].

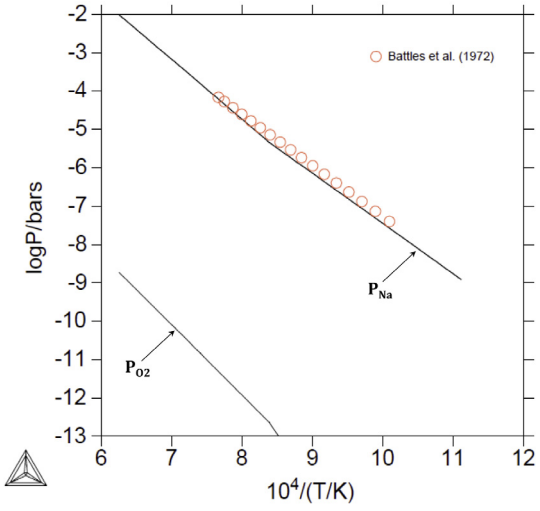

Fig. 15. Sodium and oxygen partial pressures calculated in the ternary phase field $NaUO_3$-Na_2UO_4-Na_4UO_5 and comparison with literature data [86].

$$\gamma_{acoustic} = -\frac{2}{3} - \frac{1}{2} V \frac{d}{dV} ln\left(\frac{d^2 E_{cohesive}(V)}{dV^2}\right) \quad (16)$$

$$\gamma_{optic} = \frac{1}{2} V \frac{d}{dV} ln\left(\frac{d^2 E_{cohesive}(V)}{dV^{2/3}}\right) \quad (17)$$

The volume V is calculated iteratively for a given pressure and temperature, knowing $E_{cohesive}(V)$ and the vibration frequencies at Γ point, as well as the Poisson ratio σ^0 for the crystal to zero static pressure. From $F(T,V)$ and pV we can calculate the entropy $S = -(dF/dT)_V$, the internal energy $U = F + TS$, the heat capacity at constant volume $C_V = (dU/dT)_V$, the bulk modulus $B = -V(dp/dV)_T$, and the heat capacity at constant pressure $C_p = C_V + TVB\alpha^2$.

3.2.2. Results

Our calculations were performed using the CASTEP code [90], which solves the electronic Schrödinger equation for a compound with a periodic lattice within the electronic density functional (DFT) theory using a plane-wave pseudo-potential method. The tightly bound core electrons are represented by non-local ultrasoft pseudo-potentials as proposed by Vanderbilt [91]. The exchange/-correlation energies are calculated using the Perdew *et al.* (PBE) form of the generalized gradient approximation [92]. Due to the presence of oxygen, the cutoff energy is taken as 410 eV throughout all the calculations. The first Brillouin zone is approximated with finite sampling of *k*-points using the Monkhorst–Pack scheme [93]. Furthermore, when the electron spins of the ions are unpaired, the calculations are carried out using polarized spins. The pentavalent uranium compounds $NaUO_3$ and α-Na_3UO_4 have an unpaired spin. In this case, the spin polarization calculation is performed based on ferromagnetic order. Ab initio calculations for compounds with hexavalent uranium, i.e., Na_4UO_5, α-Na_2UO_4, β-Na_2UO_4, α-$Na_2U_2O_7$ and β-$Na_2U_2O_7$, are non-spin-polarized.

The unit cell parameters obtained for the different sodium uranate structures at zero temperature and pressure are listed in

Table 11
Regression coefficients to fit the theoretical heat capacity data derived in this work using DFT.

Compound	$C_{p,m}$= A+ B· T+ C· T^2+ E· T^{-2}/(J· K^{-1}· mol^{-1})				T/K
	A	B	C	E	
$NaUO_3$	123.187	$6.36\cdot10^{-3}$	$1.24924\cdot10^{-6}$	$-1.42741\cdot10^{6}$	250–2000
α- Na_3UO_4	200.388	$6.82\cdot10^{-3}$	$5.24335\cdot10^{-6}$	$-2.67929\cdot10^{6}$	250–2000
Na_2UO_4	170.071	$13.21\cdot10^{-3}$	$1.12828\cdot10^{-6}$	$-2.40356\cdot10^{6}$	250–2000
$Na_2U_2O_7$	262.781	$24.12\cdot10^{-3}$	$-6.76942\cdot10^{-9}$	$-3.72174\cdot10^{6}$	250–2000
Na_4UO_5	243.746	$16.15\cdot10^{-3}$	$5.22474\cdot10^{-6}$	$-2.54119\cdot10^{6}$	250–2000

Table 11. The calculated volumes with DFT are systematically larger than the experimental data, which is a well-known behaviour related to the generalized gradient approximation form of the exchange/correlation energies.

The standard enthalpy of formation for the various compositions was obtained using Hess's law and the cohesive energy $E_{cohesive}(V)$ of the crystal calculated as a function of the static pressure or the corresponding equilibrium volume.

$$\begin{array}{ll} xNa^{crystal}+yU^{crystal}+zO_2^{gas}\rightarrow Na_xU_yO_{2z}^{crystal} & \Delta_fH_m(Na_xU_yO_{2z}^{crystal}) \\ xNa^{crystal}+yU^{crystal}+zO_2^{gas}\rightarrow xNa^{gas}+yU^{gas}+2zO^{gas} & x\Delta_fH_m(Na^{gas})+y\Delta_fH_m(U^{gas})+2z\Delta_fH_m(O^{gas}) \\ xNa^{gas}+yU^{gas}+2zO^{gas}\rightarrow Na_xU_yO_{2z}^{crystal} & -\Delta H_{atomisation}(Na_xU_yO_{2z}^{crystal}) \end{array} \quad (18)$$

From Hess law we obtain at temperature T:

$$\Delta_fH_m(Na_xU_yO_{2z}^{crystal}) = x\Delta_fH_m(Na^{gas})+y\Delta_fH_m(U^{gas})+2z\Delta_fH_m(O^{gas}) - \Delta H_{atomisation}(Na_xU_yO_{2z}^{crystal}) \quad (19)$$

where $\Delta_fH_m(Na^{gas}), \Delta_fH_m(U^{gas}), \Delta_fH_m(O^{gas})$ are known. $\Delta H_{atomisation}(Na_xU_yO_{2z}^{crystal})$ is derived from the model:

$$\Delta H_{atomisation}(Na_xU_yO_{2z}^{crystal}) = E_{cohesive}(V)+V\frac{dE_{coh}(V)}{dV}+\frac{5}{2}nNk_BT - Nk_BT\left[(\gamma_{ac}+1)\left(\frac{9}{8}x_D+3D(x_D)\right)+(\gamma_{op}+1)\sum_{j=1}^{3n-3}\left(\frac{x_j}{2}+\frac{x_j}{e^{x_j}-1}\right)\right] \quad (20)$$

Using the optimized total energy for sodium uranate oxides $E(Na_xU_yO_{2z})$ calculated using the CASTEP code for a given pressure, and the energy of pure sodium $E(Na)$, uranium $E(U)$ and oxygen $E(O)$ atoms as references, we obtain the cohesive energy $E_{cohesive}$ of the crystal as a function of the static pressure or the corresponding equilibrium volume V:

$$E_{cohesive}(V) = E(Na_xU_yO_{2z}) - xE(Na) - yE(U) - 2zE(O) \quad (21)$$

The reference atomic energy $(xE(Na)+yE(U)+2zE(O))$, which is identical for a given compound for all static pressures, can be calculated from the formation enthalpies of Na_2O, UO_2, γ-UO_3, Na, U, O gas tabulated [94] ideally at zero Kelvin, and the optimized total energies $E(Na_2O), E(UO_2)$ and $E(\gamma\text{-}UO_3)$ calculated using the CASTEP code:

$$\begin{aligned} xE(Na)+yE(U)+2zE(O) = {} & x\Delta_fH^o_m(Na^{gas})+y\Delta_fH^o_m(U^{gas}) \\ & +2z\Delta_fH^o_m(O^{gas})-\frac{x}{2}\Delta_fH^o_m(Na_2O^{crystal}) \\ & -u\Delta_fH^o_m(UO_2^{crystal})-v\Delta_fH^o_m(\gamma-UO_3^{crystal}) \\ & +\frac{x}{2}E(Na_2O^{crystal})+uE(UO_2^{crystal})+vE(UO_3^{crystal}) \end{aligned} \quad (22)$$

with $u=\left(\frac{x}{2}+3y-2z\right)$ and $v=\left(-\frac{x}{2}-2y+2z\right)$

The calculated standard enthalpies of formation are generally in good agreement with the experimental values obtained using solution calorimetry (Table 8), which gives confidence to the results obtained by the (ab initio + quasi-harmonic) approach. The agreement is very good for pentavalent $NaUO_3$ (0.3%), and very satisfactory for pentavalent Na_3UO_4 (0.5%). The values obtained for the hexavalent compounds are slightly overestimated by 1.7–2.8%. These differences are related to the electronic structure calculations of UO_2 and γ-UO_3 using the CASTEP code. For the latter compounds the calculation of cohesion energies constitutes a difficulty in itself (private communication [95]), and much efforts were necessary to calculate them [95]. We can only speculate that the calculated total energy of γ-UO_3 is probably tainted by a mistake, which is difficult to appreciate, and seems to impact all the calculated data for the hexavalent uranium compounds.

The heat capacity data calculated with the quasi-harmonic model are compared in Fig. 10 to the experimental data measured at low temperatures (T < 350 K) using adiabatic or thermal relaxation calorimetry, and to the values reported at high temperatures (T > 300 K) after derivation of the experimental enthalpy increment data. The corresponding standard heat capacity and entropy functions at 298.15 K are also listed in Table 8. The agreement with the low temperature data (T < 350 K) is reasonably good for all compositions, with a deviation below 2.4% for the heat capacity values at 298.15 K. The calculated standard entropies at 298.15 K show a tendency towards a larger overestimation (especially for α-Na_2UO_4 and α-$Na_2U_2O_7$), which is related to the definition of $S^o_m(298.15K)$, obtained by integration of $C_{p,m}/T = f(T)$ between T = 0 and 298.15 K. The heat capacity data derived at high temperatures (T > 300 K) show a regular increase and reasonable evolution, although the calculated values are slightly lower than reported experimentally.

In this work, the mathematical heat capacity functions implemented in the CALPHAD model (listed in Table 11) were obtained using a regression law in the temperature range (T = 250–2000 K), combining the experimental low temperature heat capacity data reported in the literature in the range (T = 250–350 K) with the heat capacity values obtained with the DFT and quasi-harmonic model in the range (T = 350–2000 K). We believe that our calculated values give a more reasonable estimation at high temperatures compared to the extrapolation of the experimental heat capacity functions listed in Table 10. The standard enthalpies of formation and entropies at 298.15 K measured experimentally were considered more accurate than the calculated ones, however, and therefore used as starting values for the CALPHAD optimization presented hereafter.

3.3. Thermodynamic modelling

3.3.1. Na-U binary phase diagram

To the best of our knowledge, only one experimental study has been reported in the literature on the Na-U binary system [96], and there are probably no compounds formed [97]. Uranium metal exists in three allotropic forms: orthorhombic α-U, tetragonal β-U, and cubic γ-U, with transition temperatures and melting points at $T_{tr}(\alpha\rightarrow\beta)$ = (941 ± 2) K, $T_{tr}(\beta\rightarrow\gamma)$ = (1049 ± 2) K, $T_{fus}(\gamma)$ = (1407 ± 2) K [98], respectively. Douglas found the solubility of uranium in liquid sodium at 370.8 K to be less than 0.05 wt% and

probably many times smaller [96], while uranium and sodium did not react when heated at 823 K for long periods of time [97].

Metallic Na and U were described as regular solution using the following expression:

$$G_m^{\varphi}(T) = \sum x_i G_i^{\varphi}(T) + RT\sum x_i ln x_i + x_U x_{Na} L_{U,Na}^{\varphi} \quad (23)$$

where x_i corresponds to the atomic fraction of i, $G_i^{\varphi}(T)$ the Gibbs energy of the pure species i in the phase φ, and $L_{U,Na}^{\varphi}$ the interaction parameter between U and Na in this phase.

The parameters of Dinsdale, also adopted for the TAF-ID database, were used to model pure uranium [40]. Na and U metal were assumed to be immiscible in the present work. Large positive values were thereafter assigned to the interaction parameters $L_{U,Na}^{\varphi}$ as listed in Table 6.

3.3.2. Liquid

To describe the composition variation from a metallic liquid (Na,U) to an oxide liquid (Na,U,O), U^{4+} cations were added to the ionic two-sublattice model.

$$(U^{4+}, Na^{+})_P (O^{2-}, Na_2O_2, Va^{Q-}, O)_Q \quad (24)$$

where P and Q are equal to the average charge of the opposite sublattice:

The Gibbs energy of the liquid phase is given by the following expression:

$$G^{liq} = {}^{ref}G^{liq} + {}^{id}G^{liq} + {}^{ex}G^{liq} \quad (25)$$

$${}^{ref}G^{liq} = \sum_C \sum_A y_C y_A {}^{o}G^{liq}_{(C)(A)} + Q y_{Va} \sum_C y_C {}^{o}G^{liq}_{C} + Q \sum_B y_B {}^{o}G^{liq}_{B} \quad (26)$$

$${}^{id}G^{liq} = RT\left[P\sum_C y_C ln y_C + Q\left(\sum_A y_A ln y_A + y_{Va} ln y_{Va} + \sum_B y_B ln y_B\right)\right] \quad (27)$$

$${}^{ex}G^{liq} = \sum_{C_1}\sum_{C_2}\sum_A y_{C_1} y_{C_2} y_A L^{liq}_{(C_1,C_2)(A)} + \sum_{C_1}\sum_{C_2} y_{C_1} y_{C_2} y_{Va}^2 L^{liq}_{(C_1,C_2)(Va)} \quad (28)$$

$$+ \sum_C \sum_{A_1}\sum_{A_2} y_C y_{A_1} y_{A_2} L^{liq}_{(C)(A_1,A_2)} + \sum_C \sum_A y_C y_A y_{Va} L^{liq}_{(C)(A,Va)} \quad (29)$$

$$+ \sum_C \sum_A \sum_B y_C y_A y_B L^{liq}_{(C)(A,B)} + \sum_C \sum_B y_C y_B y_{Va} L^{liq}_{(C)(Va,B)} \quad (30)$$

$$+ \sum_{B_1}\sum_{B_2} y_{B_1} y_{B_2} L^{liq}_{(B_1,B_2)} \quad (31)$$

where A is an anion, C a cation and B a neutral species. ${}^{o}G^{liq}_{(C)(A)}$ corresponds to the Gibbs energy of $(v_C + v_A)$ moles of liquid Cv_AAv_C, ${}^{o}G^{liq}_{(C)}$ is the Gibbs energy of the liquid phase for the pure element corresponding to the C cation and ${}^{o}G^{liq}_{B}$ the Gibbs energy of the liquid phase for the neutral species B.

The parameters relative to the $(U^{4+})_P(O^{2-}, Va^{Q-}, O)_Q$ oxide liquid phase in the U-O system were taken from the work of Guéneau et al. [13]. Metallic liquid Na and U were assumed to be immiscible as discussed previously, so that a large interaction parameter $L^{liq}_{(U^{4+},Na^{+})(Va)}$ was assigned between uranium and sodium metal as listed in Table 6. No ternary interaction parameters were introduced in the absence of experimental information on the ternary liquid phase.

3.3.3. Non stoichiometric uranium dioxide $UO_{2\pm x}$

UO_2 adopts a fluorite type lattice with a marked ionic character and a wide homogeneity range [13,99]. $UO_{2\pm x}$ was described using the compound energy formalism with ionic species as recommended in [13].

$$(U^{3+}, U^{4+}, U^{5+})(O^{2-}, Va)_2 (O^{2-}, Va) \quad (32)$$

We refer the reader to the latter work [13] for further description of the model and optimized enthalpy, entropy, and interaction parameters for this phase.

3.3.4. Stoichiometric compounds

U_4O_9, U_3O_8, UO_3, Na_2UO_4, Na_4UO_5, $Na_2U_2O_7$, $NaUO_3$, and Na_3UO_4 were described as stoichiometric compounds in this work. The temperature dependence of the molar Gibbs energy G_m^{φ} for one mole of formula unit is described by a power series in temperature as follows:

$$G_m^{\varphi}(T) - \sum_i n_i^{\varphi} {}^{o}H_i^{SER}(298.15\ K) = a + b\cdot T + c\cdot T\cdot lnT + \sum d_n T^n \quad (33)$$

where n_i^{φ} is the number of atoms of the ith element in the oxide formula. The coefficients a, b, c and d_n for the uranium oxides are listed in the work of [13]. Those for the sodium uranates were derived using the enthalpies of formation, entropies, and transition enthalpies measured experimentally (Table 8), and the heat capacity functions obtained after regression of the DFT and quasi-harmonic model data (Table 11). The enthalpies of formation and entropies were further optimized in this work as described below.

3.3.5. Gas

The gas phase was described by an ideal mixture of (U, UO, UO_2, UO_3, Na, Na_2, Na_2O, O, O_2, O_3) gaseous species. The Gibbs energy is expressed by:

$$G^{\varphi} = \Sigma_i y_i {}^{o}G_i^{\varphi} + RT\sum_i y_i ln y_i + RTlnP/P^{o} \quad (34)$$

where y_i is the fraction of the species i in the gas phase. ${}^{o}G_i^{\varphi}$ represents the standard Gibbs energy of the gaseous species i. P^{o} is the standard pressure. The Gibbs energy functions for U(g), UO(g), UO_2(g), UO_3(g) were taken from the recent reviews by [63,64]. Those for Na(g), Na_2(g), Na_2O(g), O(g), O_2(g), O_3(g) were taken from the SGTE database [62].

3.4. Optimized Na-U-O thermodynamic model

The Na-U-O ternary phase diagrams calculated at (T = 300, 700, 900, 1350, 1400, 1750, 2350, 2500 and 2550 K) are shown in Figs. 11a,b,c,d,12, 11e,f, B1a and b. Temperatures are expected to reach 773–1373 K at the pellet edge of SFRs [100], and the phase equilibria in this range of temperatures are therefore particularly relevant for the safety assessment of the SFR.

The calculated phase boundaries between the ternary phase fields are in good agreement with the predictions of Blackburn [9] except for those involving the Na_3UO_4 phase. The authors suggested three-phase equilibria between UO_2-$NaUO_3$-Na_3UO_4 and $NaUO_3$-Na_3UO_4-Na_4UO_5 (dotted line in Fig. 12), whereas the calculation predicts three-phase equilibria between UO_2-$NaUO_3$-Na_4UO_5 and UO_2-Na_3UO_4-Na_4UO_5. The latter phase boundaries are in fact in better agreement with the results of Smith et al. on the trisodium uranate phase [66]. When mixing sodium oxide with uranium oxide in a (2.1:1) ratio and heating under argon at 1273 K for 24 h, the authors obtained a phase mixture corresponding to 21.8 wt% UO_2 + 78.2 wt% $\alpha - Na_{3.16(2)}U_{0.84(2)}O_4$ [66], which is found within the three-phase field UO_2-Na_3UO_4-Na_4UO_5 as shown in Fig. 12.

The standard entropy functions of $NaUO_3$ and α-Na_2UO_4, enthalpy of formation of α-Na_2UO_4 at 298.15 K, and enthalpy of transition of α-$Na_2U_2O_7$ were optimized in this work to fit the sodium partial pressures measured experimentally in the $NaUO_3$-$Na_2U_2O_7$-UO_2 [68] and $NaUO_3$-Na_2UO_4-$Na_2U_2O_7$ [88] phase fields: $\Delta_f H_m^{o}(\alpha\text{-}Na_2UO_4, cr, 298.15\ K) = -1901.2\ kJ{\cdot}mol^{-1}$,

Table 12
Decomposition reactions and temperatures of the sodium uranates calculated in the present model (A for $P_{tot} = 10^5$ Pa; B for n(He) = 0.016 mol), and measured experimentally (KEMS=Knuden effusion mass spectrometry under high vacuum conditions at a pressure $P = (5{\cdot}10^{-6} \pm 4{\cdot}10^{-6})$ Pa; HTXRD=High temperature X-ray diffraction measurements under helium atmosphere at a pressure $P_{He} = (0.065 \pm 0.015)$ MPa in a furnace chamber of volume 0.5 L.

CALPHAD calculation (closed system)		Experimental data (open system)		
Decomposition reaction	T/K	Decomposition reaction	T[a]/K	Ref.
$2NaUO_3 = Na_2UO_4 + UO_2$	1701.9[A]	$3NaUO_3 = Na_2U_2O_7 + UO_2 + Na(g)$	1550	KEMS,HTXRD [65,68]
$3NaUO_3 = Na_2U_2O_7 + UO_2 + Na(g)$	1645.6[B]			
$2Na_3UO_4 = Na_4UO_5 + UO_2 + 2Na(g) + 1/2O_2(g)$	1358.3[A] 944.4[B]	$Na_3UO_4 = NaUO_3 + 2Na(g) + 1/2O_2(g)$	1173	HTXRD [69]
$Na_4UO_5 = Na_2UO_4 + 2Na(g) + 1/2O_2(g)$	2341.6[A] 1756.3[B]	$Na_4UO_5 = NaUO_3 + 3Na(g) + O_2(g)$	>1273	HTXRD [65]
$Na_2UO_4 = UO_2 + 2Na(g) + O_2(g)$	2532.4[A]			
$2Na_2UO_4 = Na_2U_2O_7 + 2Na(g) + 1/2O_2(g)$	1827.1[B]			
$Na_2U_2O_7 = Na_2UO_4 + UO_2 + 1/2O_2(g)$	2476.2[A]	$Na_2U_2O_7 = 2UO_2 + 2Na(g) + 3/2O_2(g)$	1620	KEMS [68]
$Na_2U_2O_7 = 2UO_2 + 2Na(g) + 3/2O_2(g)$	1913.4[B]			

[a]Standard uncertainties u are $u(T) = 20$ K for HTXRD data, $u(T) = 10$ K for KEMS data.

$S^o_m(\alpha\text{-}Na_2UO_4, cr, 298.15\ K) = 170.0\ J{\cdot}K^{-1}{\cdot}mol^{-1}$, $S^o_m(NaUO_3, cr, 298.15\ K) = 127.0\ J{\cdot}K^{-1}{\cdot}mol^{-1}$, $\Delta_f H^o_m(\alpha\text{-}Na_2U_2O_7, cr, 600\ K) = 2.8\ kJ{\cdot}mol^{-1}$.

The recent Knudsen effusion mass spectrometric studies of Smith *et al.* in the $NaUO_3$-$Na_2U_2O_7$-UO_2 phase field [68] have questioned the reported value for the standard entropy of $NaUO_3$. The authors found a poor agreement between second law and third law analysis of their data, and attributed the discrepancy to the latter function. They derived $S^o_m(NaUO_3, cr, 298.15\ K) = 126.4\ J{\cdot}K^{-1}{\cdot}mol^{-1}$, which is about $6\ J{\cdot}K^{-1}{\cdot}mol^{-1}$ lower than the value reported by [101] using low temperature adiabatic calorimetry, i.e., $(132.8 \pm 0.4)\ J{\cdot}K^{-1}{\cdot}mol^{-1}$. The former value, like the one derived from the present optimization, are in better agreement with the additive rule using the data of UO_2 [64], UO_3 [64] and Na_2O [24] ($124.1\ J{\cdot}K^{-1}{\cdot}mol^{-1}$). The optimized value for the enthalpy of formation of α-Na_2UO_4 is within experimental uncertainties. The optimized standard entropy for the latter compound, $S^o_m(\alpha\text{-}Na_2UO_4, cr, 298.15\ K) = 170.0\ J{\cdot}K^{-1}{\cdot}mol^{-1}$, is in very good agreement with the trend shown by the series of alkali and alkaline-earth uranates A_nUO_4 (A = Mg, Sr, Ba, Cs) [102–105]. Previous studies by Popa *et al.* [102] and Konings *et al.* [103] have evidenced a regular evolution as a function of the ionic radius of the alkali and alkaline earth cation, and the value predicted from this trend is $169.9\ J{\cdot}K^{-1}{\cdot}mol^{-1}$ [105]. Finally, the small value of the transition enthalpy of $Na_2U_2O_7$ at 600 K reflects the fact that the α and β forms have closely related structures.

Using those optimized functions, the present model reproduces very well the partial pressure data of Smith et *al.* in the $NaUO_3$-$Na_2U_2O_7$-UO_2 phase field [68] and Pankajavelli *et al.* in the $NaUO_3$-Na_2UO_4-$Na_2U_2O_7$ phase field [88] as shown in Figs. 13 and 14. The data of Jayanthi *et al.* [87] are of the same order of magnitude as the calculation, but the slope of the sodium partial pressure is much steeper (Fig. 14). This feature is also reflected in their second and third law results for the enthalpy of formation of $NaUO_3$(cr), i.e., $-(1481.4 \pm 13.4)\ kJ{\cdot}mol^{-1}$ and $-(1476.7 \pm 13.4)\ kJ{\cdot}mol^{-1}$, respectively, which are only in moderate agreement and about $15\ kJ{\cdot}mol^{-1}$ lower than the recommended value. The partial pressures measured by Battles *et al.* [86] are subject to a rather large uncertainty as detailed in the work of [104]. We have preferred not to optimize the thermodynamic functions of the sodium uranates based on the latter data and recommend repeating those measurements. The reported partial pressures in $NaUO_3$-Na_2UO_4-$Na_2U_2O_7$ phase field are lower than reported by [88,87], and calculated herein. The sodium partial pressures reported in the $NaUO_3$-Na_4UO_5-Na_2UO_4 phase field are in very good agreement with the calculation, without further optimizing the thermodynamic functions of Na_4UO_5, but this situation might be fortuitous. Moreover, the authors reported partial pressures for the $NaUO_3$-Na_3UO_4-Na_4UO_5 and $NaUO_3$-Na_3UO_4-UO_2 phase fields, but the latter are not stable according to the present thermodynamic model.

The decomposition temperatures and decomposition mechanisms of the sodium uranate ternary compounds are not known precisely to this date. These can only be roughly estimated as listed in Table 12 based on the Knudsen effusion mass spectrometry measurements of [68,69] under high vacuum conditions ($P = 10^{-7}$–10^{-8} mbar), and high temperature X-ray diffraction (HTXRD) measurements of [65] under helium atmosphere (P_{He} = 500–800 mbar in a furnace chamber of volume 0.5 L). Those are compared in Table 13 to the decomposition reactions and temperatures calculated from the thermodynamic model under standard conditions ($P_{tot} = 1$ bar) and in the presence of He gas ($n(He) = 0.016$ mol), simulating the conditions in the HTXRD experiments. The hexavalent phases Na_4UO_5, $Na_2U_2O_7$, Na_2UO_4 are the most stable according to these calculations, which is also reflected in the experimental results. The more reducing conditions in the presence of He gas results in a significant lowering of the decomposition temperatures, and a different decomposition mechanism for $NaUO_3$, Na_2UO_4 and $Na_2U_2O_7$ compared to the standard conditions.

The calculated decomposition mechanisms are the same as observed experimentally for $NaUO_3$ and $Na_2U_2O_7$, but they lead to different decomposition products for Na_3UO_4 and Na_4UO_5. The comparison is not ideal as the calculations refer to a closed system, in other words they are computed at fixed composition, whereas the KEMS or HTXRD experiments correspond to open systems where weight losses occur, meaning that the compositions change during the measurements. Looking at the calculated three-phases equilibria in the Na-U-O system, one can nevertheless predict the evolution of the samples by effusion and compare the prediction with the experimental observations. According to the calculations, $NaUO_3$ evolves by effusion and loss of Na(g) in the ternary phase field UO_2-$Na_2U_2O_7$-$NaUO_3$ until all $NaUO_3$ has disappeared, in good agreement with the KEMS and HTXRD results of [65,68]. When it looses $\{2Na(g)+3/2O_2(g)\}$, $Na_2U_2O_7$ evolves on the pseudo-binary section UO_2-$Na_2U_2O_7$ until only uranium dioxide remains, as observed in the KEMS studies of [68]. Furthermore, Na_4UO_5 evolves by effusion and loss of $\{3Na(g)+O_2(g)\}$ on the pseudo-binary section Na_4UO_5-$NaUO_3$, as observed in the HTXRD studies of [65]. Finally, Na_3UO_4 evolves by effusion and loss of $\{2Na(g)+1/2O_2(g)\}$ in the ternary phase field Na_3UO_4-Na_4UO_5-UO_2 until all Na_3UO_4 has disappeared, and only Na_4UO_5 and UO_2 remain. Na_4UO_5 subsequently decomposes to $NaUO_3$ by effusion as described previously. In the HTXRD experiment of [69], only $NaUO_3$ is observed as remaining product as the decomposition is too fast during the heating ramp to vizualise the intermediate decomposition product Na_4UO_5.

Finally, it is worth pointing out that the calculated decomposition temperatures in the presence of He are of the same order of magnitude as observed experimentally, and respect the observed relative stabilities ($Na_2U_2O_7$ > Na_4UO_5 > $NaUO_3$ > Na_3UO_4). Further experimental investigations of the ternary phase fields, and decomposition temperatures of the ternary compounds would finally be extremely beneficial to confirm the predicted stable phase boundaries in this system and refine the present model above $T \sim 1700$ K.

4. Margin to the safe operation of SFRs

Based on the thermodynamic assessment of the Na-U-O system, the oxygen potential thresholds required for the formation of the sodium uranate phases are calculated and compared to the oxygen levels expected in the sodium coolant. Such calculations are essential if one wants to predict the consequences of the nuclear fuel-sodium interaction in a Sodium-cooled Fast reactor.

4.1. Oxygen potential thresholds of formation

The condition of occurrence of the reaction between fuel and sodium is dictated by the amount of oxygen available within the nuclear fuel and liquid sodium. This is expressed by the equilibrium thermodynamic oxygen potential $\Delta\overline{G}_{O_2}^{eq}$ for the three-phase region containing liquid sodium, urania (respectively urania–plutonia), and sodium uranate (respectively urano-plutonate) [4–8]. The latter oxygen potential can be expressed either in terms of oxygen-to-metal ratio in the oxide phase O/M, plutonium valency in the MOX fuel V_{Pu}, or in terms of oxygen concentration C_O^{eq} in the liquid sodium [4–8]. Mignanelli and Potter [8], and Adamson et al. [4] reported that the threshold oxygen potentials for the formation of Na_3MO_4 ($M = U,U_{1-\alpha}Pu_\alpha$) were very similar for the ternary Na-U-O and quaternary Na-U-Pu-O systems. The authors showed that the contact between the metallic coolant and the urania–plutonia solid solution leads to an oxygen concentration increase in the liquid sodium in conjunction with the reduction to a lower valency of the plutonium in the oxide phase.

Stoichiometric uranium dioxide $UO_{2.00}$ is stable relative to liquid sodium, but hyperstoichiometric UO_{2+x} can react, which can be expressed as follows [8,4]:

$$Na(l) + O_2(g) \rightarrow Na(l, O \text{ in sln}) \quad (35)$$

$$3xNa(l, O \text{ in sln}) + 2UO_{2+x}(cr) \rightarrow xNa_3UO_4(cr) + (2-x)UO_{2.00}(cr) \quad (36)$$

corresponding to the equilibrium reaction:

$$3Na(l, O \text{ in sln}) + UO_2(cr) + O_2(\text{dissolved in Na or oxide}) \rightleftharpoons Na_3UO_4(cr) \quad (37)$$

Considering the sodium quasi-pure, with very little oxygen dissolved, the partial Gibbs energy of sodium $\Delta\overline{G}_{Na}$ is taken to be zero, and the equilibrium oxygen potential for this reaction is given by:

$$\Delta\overline{G}_{O_2}^{eq}(T) = RTln(P_{O_2}/P^o) = \Delta_f G_m^o(Na_3UO_4, cr, T) - \Delta_f G_m^o(UO_2, cr, T) \quad (38)$$

where P_{O_2} is the pressure of oxygen, P^o the standard partial pressure equal to 1 bar, $\Delta_f G_m^o(Na_3UO_4, cr, T)$ and $\Delta_f G_m^o(UO_2, cr, T)$ the Gibbs energies of formation of Na_3UO_4 and UO_2, respectively, R the universal gas constant, and T the temperature.

Using the thermodynamic functions of the present CALPHAD model for α-Na_3UO_4, and the most recent updates for the thermodynamic functions of UO_2 [64], the calculation performed in the temperature range (600–1200 K) yields $\Delta\overline{G}_{O_2}^{eq}(T/K) = -948630 + 263.28T$ J·mol^{-1}, which is very close to the equation established by Adamson et al. in 1981 $\Delta\overline{G}_{O_2}^{eq}(T/K) = -944951 + 261.34T$ J·molX^{-1}.

Table 13
Oxygen potential thresholds of formation in the temperature range 600–1200 K.

Compound	$\Delta\overline{G}_{O_2}^{eq}$(T/K) (J·mol^{-1})
α-Na_3UO_4	$-948630 + 263.28T$
$NaUO_3$	$-827396 + 225.16T$
α-Na_2UO_4	$-821463 + 229.64T$
Na_4UO_5	$-921285 + 247.31T$
$Na_2U_2O_7$	$-689968 + 197.62T$
α-$Na_{3.16}U_{0.84}O_4$	$-926000 + 246.48T$

The oxygen potential thresholds were also estimated for $NaUO_3$, α-Na_2UO_4, Na_4UO_5, and $Na_2U_2O_7$, using the thermodynamic functions optimized in the CALPHAD model. The derived equations are listed in Table 13.

Finally, the calculation was also performed for the mixed valence state composition $Na_{3.16}U_{0.84}O_4$. The necessary thermodynamic functions, i.e. enthalpy of formation, entropy, and heat capacity, were approximated, supposing an ideal behaviour, with a linear combination of the thermodynamic functions of Na_3UO_4 and Na_4UO_5 as detailed in Appendix A. The associated equilibrium reaction is:

$$3.16Na(l) + 0.84UO_2(cr) + 1.16O_2(dissolved) \rightleftharpoons Na_{3.16}U_{0.84}O_4(cr) \quad (39)$$

and the derived oxygen potential is $\Delta\overline{G}_{O_2}^{eq}(T/K) = -926000 + 246.48T$ J·mol^{-1}. The obtained oxygen potential lines are shown in Fig. 16.

4.2. Oxygen levels in liquid sodium

The oxygen potential, which corresponds to the threshold for the onset of the reaction between fuel and sodium, should be compared with the concentration levels of oxygen dissolved in liquid sodium. The relationship between the two is defined by the oxygen solubility equation as a function of temperature on the one hand, and by the Gibbs energy of formation of sodium oxide on the other hand [4]. Sodium oxide forms when the solubility limit of oxygen in sodium is reached:

$$2Na(l) + \frac{1}{2}O_2(g) \rightleftharpoons Na_2O(diss) \quad (40)$$

The Na_2O saturation corresponds to an oxygen concentration of the order of 6000 wppm [76,106], which is, however, well above the normal operating conditions of SFRs (where oxygen levels are kept below circa 3 wppm [106] to avoid corrosion issues of the containment material [14]).

At equilibrium, the following relationship holds:

$$2\mu_{Na} + \frac{1}{2}\mu_{O_2} = \mu_{Na_2O} = G_m^o(Na_2O) + RTlna_{Na_2O} \quad (41)$$

with μ_{Na}, μ_{O_2} and μ_{Na_2O} the chemical potentials of liquid sodium, oxygen, and sodium oxide, respectively, and a_{Na_2O} the activity of Na_2O in liquid sodium.

Taking liquid sodium as the reference state, and considering that the oxygen levels are very low, $\Delta\overline{G}_{Na}$ can be approximated to be zero. The activity of Na_2O is expressed assuming that Henry's law is obeyed:

$$a_{Na_2O} = \frac{C_{Na_2O(dissolved)}}{C_{Na_2O(saturated)}} = \frac{C_{O_2}}{C_{O_2,s}} \quad (42)$$

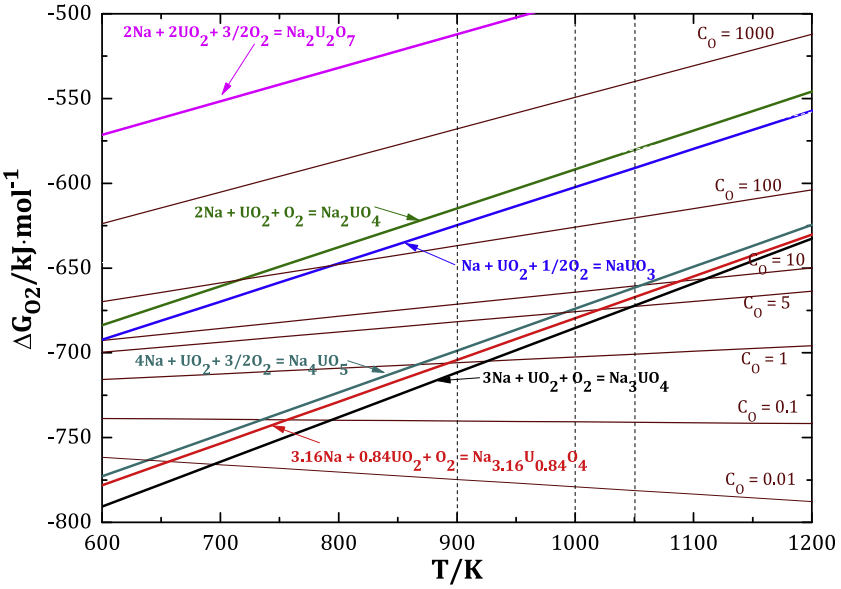

Fig. 16. Calculated oxygen potential thresholds for the formation of Na-U-O ternary phases, and comparison with the oxygen levels in liquid sodium (C_0 from 0.01 to 1000 wppm), considering the solubility equation of Noden [36].

with C_{O_2} the concentration of oxygen dissolved in liquid sodium and $C_{O_2,s}$ the concentration of oxygen at saturation, both expressed in wppm (weight ppm). After substitution into Eq. (41), we obtain the general expression:

$$\Delta\overline{G_{O_2}^{eq}}(T) = 2\Delta_f G_m^o(Na_2O) + 2RTln\frac{C_{O_2}}{C_{O_2,s}} \quad (43)$$

The calculation leads to $\Delta\overline{G_{O_2}^{eq}}(T/K) = -735691.3 + (33.232 + 38.287 log C_O)T$ J·mol^{-1} using the solubility data of Noden [36,37]. Those oxygen potential lines are drawn in Fig. 16 for oxygen levels C_O in sodium ranging from 0.1 wppm to 1000 wppm, together with the oxygen potential required for the formation of the various sodium uranate phases.

4.3. Discussion

The temperature on the surface of a fuel rim in a SFR is in the range 893 to 923 K, while it may exceed 2273 K at the centre [3]. The temperature range where the fuel-sodium reaction product is susceptible to form is 893–1373 K [100]. From Fig. 16, we deduce that an oxygen concentration of about 0.7 wppm is sufficient at 900 K for the formation of α-Na_3UO_4, while an oxygen concentration of 3 wppm is necessary at 1000 K (5 wppm at 1050 K). The latter values are in the typical operating range of SFRs, which is why it is essential to fully understand the physical and chemical properties of the sodium uranate and urano-plutonate products. The results are the same using the recommended data of Eichelberg [33]. With the data of Claxton, we find circa 0.3 wppm at 900 K, 1.2 wppm at 1000 K, and 2 wppm at 1050 K.

It is interesting to compare these results with those of Smith [107] who measured directly the oxygen concentrations in sodium in equilibrium with $U_{0.75}Pu_{0.25}O_2$, and in sodium at the three phases field Na-MO_{2-x}-Na_3MO_4 (M=$U_{1-z}Pu_z$) by the vanadium equilibration method in the temperature range 923–1173 K. Smith found oxygen concentrations ranging from 0.1 to 0.4 wppm, which is slightly lower than calculated herein, but in fair agreement.

Looking at other sodium uranate compositions, we observe that the oxygen thresholds are much higher: above 1000 wppm for $Na_2U_2O_7$, between 100 and 1000 wppm for $NaUO_3$ and α-Na_2UO_4 in the temperature range 900–1050 K. Surprisingly, the oxygen threshold for hexavalent Na_4UO_5 (about 1.5 wppm at 900 K, 5.5 wppm at 1000 K, and 10 wppm at 1050 K) is very close to the one for pentavalent Na_3UO_4, and below the one for pentavalent $NaUO_3$. The threshold for the $Na_{3.16(2)}U_{0.84(2)}O_4$ compound synthesized by [66] is between that of Na_3UO_4 and Na_4UO_5. It is closer to the threshold of Na_4UO_5 around 600 K, but approaches the one of Na_3UO_4 with increasing temperature. These results have to be related to the structural similarities between the Na_3UO_4 and Na_4UO_5 end-members, which are both derived from a NaCl type of structure. The present calculation shows that relatively low oxygen concentrations in liquid sodium can also lead to the formation of U (VI) phases within the fuel, which was never considered in past studies. The consequences (in terms of corrosion, thermal expansion behaviour, etc) need to be considered for a thorough safety assessment of the sodium fuel interaction.

5. Conclusions

A thermodynamic model for the Na-O system is reported, which is consistent with the experimental data available on this system as reviewed by Wriedt [14]. The model reproduces the oxygen solubility limit determined by Noden [36], the phase transitions and melting temperatures of sodium and its oxides, as well as the suggested monotectic and eutectic equilibria. The present DSC measurements moreover argue for the existence of a {Na_2O-I + Na_2O_2-II = liquid} eutectic equilibrium at 843 K as anticipated by Wriedt [14].

A CALPHAD model for the Na-U-O system was also developed, which is particularly relevant for the safety assessment of the sodium-fuel chemical interaction in SFRs. The calculations predict slightly different stable phase boundaries than reported in the literature. In particular, the three-phases equilibria UO_2-Na_3UO_4-

Na_4UO_5 is suggested, which is consistent with the results recently obtained by Smith et al. [66]. Ab-initio calculations combined with a quasi-harmonic model were performed, which have allowed to derive the standard enthalpies of formation, standard entropies, and heat capacity functions of the sodium uranate compounds. The heat capacity data derived with this method at high temperatures were implemented in the CALPHAD model for this system, as for most phases experimental measurements are limited to $T \sim 1000$ K, and cannot be extrapolated with sufficient confidence at high temperatures. The CALPHAD model was moreover optimized to fit the sodium partial pressures measured in the ternary phase fields $NaUO_3$-$Na_2U_2O_7$-UO_2 and $NaUO_3$-Na_2UO_4-$Na_2U_2O_7$. The optimized thermodynamic functions for $NaUO_3$ and α-Na_2UO_4 are in good agreement with literature data.

Finally the oxygen potential thresholds required for the formation of the sodium uranate phases from liquid sodium and hyperstoichiometric urania were determined in this work. This potential was estimated as $\Delta\overline{G_{O_2}^{eq}}(T/K) = -948630 + 263.28T$ J·mol^{-1} for α-Na_3UO_4, which corresponds to oxygen levels of 0.7 wppm in liquid sodium at 900 K, and 3 wppm at 1000 K. The latter levels being typically encountered in SFRs, it is crucial from a safety perspective to have a thorough knowledge of the Na_3UO_4 reaction product. The oxygen thresholds for the $\alpha - Na_{3.16(2)}U_{0.84(2)}O_4$ and Na_4UO_5 phases were found very close to the latter values (around 1.5 wppm at 900 K and 5.5 wppm at 1000 K), which must be related to the structural similarities between the Na_3UO_4 and Na_4UO_5 end members. This suggests that low oxygen concentrations in liquid sodium can also lead to the formation of U(VI) within the fuel, which was not anticipated in past studies. These results have evident consequences from safety perspectives, and should be considered in the computer codes simulating an accidental event scenario from the initiating event to the potential release of radioactive elements into the environment.

Appendix A. Thermodynamic functions of $\alpha - Na_{3.16(2)}U_{0.84(2)}O_4$

The thermodynamic functions of $Na_{3.16(2)}U_{0.84(2)}O_4$ at 298.15 K were approximated using a linear combination of the functions of Na_3UO_4 and Na_4UO_5 supposing an ideal behaviour:

$$\begin{aligned}\Delta_f H_m^o(Na_{3.16}U_{0.84}O_4) &= 0.2\Delta_f H_m^o(Na_3UO_4) + 0.8\Delta_f H_m^o(Na_{3.2}U_{0.8}O_4)\\ &= 0.2\Delta_f H_m^o(Na_3UO_4) + 0.64\Delta_f H_m^o(Na_4UO_5) \qquad (A.1)\\ S_m^o(Na_{3.16}U_{0.84}O_4) &= 0.2S_m^o(Na_3UO_4) + 0.8S_m^o(Na_{3.2}U_{0.8}O_4) + S_{mix}^o\\ &= 0.2S_m^o(Na_3UO_4) + 0.64S_m^o(Na_4UO_5) + S_{mix}^o \qquad (A.2)\end{aligned}$$

where S_{mix}^o is a configurational entropy term equal to $-R(0.2ln0.2 + 0.8ln0.8)$, and R the gas constant.

The calculation yielded: $\Delta_f H_m^o(Na_{3.16}U_{0.84}O_4, cr, 298.15\ K) = -(1977.3 \pm 2.1)$kJ·mol^{-1}, and $S_m^o(Na_{3.16}U_{0.84}O_4, cr, T)$=(202.2 ± 4.7) J·K^{-1}·mol^{-1}.

The heat capacity of $Na_{3.16(2)}U_{0.84(2)}O_4$ was estimated using Neumann–Kopp's rule:

$$C_{p,m}^o(Na_{3.16}U_{0.84}O_4) = 0.2C_{p,m}^o(Na_3UO_4) + 0.64C_{p,m}^o(Na_4UO_5) \qquad (A.3)$$

which yielded:

$$C_{p,m}^o(Na_{3.16}U_{0.84}O_4, cr, T)/(J\cdot K^{-1}\cdot mol^{-1}) = 196.075 + 1.17\cdot 10^{-2}\cdot T + 4.39250\cdot 10^{-6}\cdot T^2 - 2.16222\cdot 10^6\cdot T^{-2} \qquad (A.4)$$

$$C_{p,m}^o(Na_{3.16}U_{0.84}O_4, cr, 298.15K)/(J\cdot K^{-1}\cdot mol^{-1}) = (175.6 \pm 4.2) \qquad (A.5)$$

Appendix B. Na-U-O ternary phase diagram

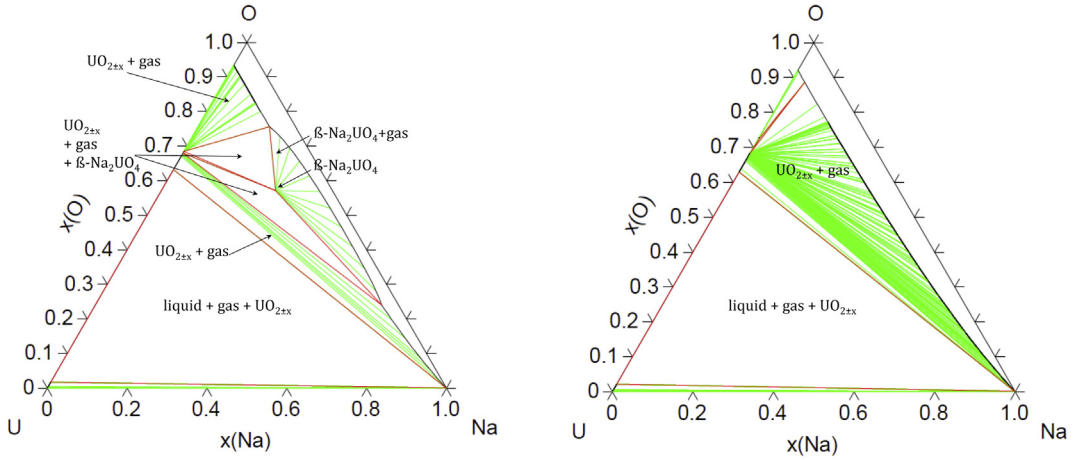

(a) T=2500 K (b) T=2550 K

Fig. B1. Calculated Na-U-O phase diagrams at T = 2500 K and T = 2550 K and 1 bar.

References

[1] GIF (Generation IV International Forum). Technical report, 2013.
[2] GIF (Generation IV International Forum). Technical report, 2014.
[3] Y. Guerin, in: R.J.M. Konings, T.R. Allen, R.E. Stoller, S. Yamanaka (Eds.), Comprehensive Nuclear Materials, Vol. 2, Chapter 2.21: Fuel Performance of Fast Spectrum Oxide Fuel, Elsevier, 2012, pp. 547–578.
[4] M.G. Adamson, M.A. Mignanelli, P.E. Potter, M.H. Rand, J. Nucl. Mater. 97 (1981) 203–212.
[5] M.A. Mignanelli, P.E. Potter, J. Nucl. Mater. 114 (1983) 168–180.
[6] M.A. Mignanelli, P.E. Potter, J. Nucl. Mater. 125 (1984) 182–201.
[7] M.A. Mignanelli, P.E. Potter, J. Nucl. Mater. 130 (1985) 289–297.
[8] M.A. Mignanelli, P.E. Potter, Thermochim. Acta 129 (1988) 143–160.
[9] P.E. Blackburn. In International Atomic Energy Agency, Proceedings of a Panel on the Behaviour and Chemical State of Irradiated Ceramic Fuels, Organized by International Atomic Energy Agency and Held in Vienna, 7–11 August 1972, IAEA, Vienna, (1974) 393–410.
[10] M. Housseau, G. Dean, F. Perret, In Panel Proceedings Series, IAEA, page 349, IAEA, Vienna, 1974.
[11] M. Housseau, G. Dean, J.-P. Marcon, and J.F. Marin, Report CEA-N-1588 (Commissariat à l'énergie atomique et aux énergies alternatives), 1973.
[12] H.L. Lukas, S.G. Fries, B. Sundman, Computational Thermodynamics, Cambridge University Press, The Calphad method, 2007.
[13] C. Guéneau, N. Dupin, B. Sundman, C. Martial, J.-C. Dumas, S. Gossé, S. Chatain, F. De Bruycker, D. Manara, R.J.M. Konings, J. Nucl. Mater. 419 (1–3) (2011) 145–167.
[14] H.A. Wriedt, Bull. Alloy Phase Diagrams 8 (3) (1987) 234–246.
[15] G.A. Sullivan, J.W. Weymouth, Phys. Rev. A 136 (4) (1964) A1141–A1148.
[16] E. Zintl, A. Harder, B. Dauth, Z. Elektrochem. 40 (8) (1934) 588–593.
[17] H. Föppl, Z. Anorg. Chem. 291 (1957) 12–50.
[18] R.L. Tallman, Diss. Abstr. 20 (1960) 4293.
[19] M. Ziegler, M. Rossenfeld, W. Kánzig, P. Fischer, Helv. Phys. Acta 49 (1) (1976) 57–90.
[20] G.F. Carter, D.H. Templeton, J. Am. Chem. Soc. 75 (1953) 1229–1231.
[21] D.H. Templeton, C.H. Dauber, J. Am. Chem. Soc. 72 (1950) 2251–2254.
[22] W. Klein, K. Armbruster, M. Jansen, Chem. Commun. 6 (1998) 707–708.
[23] W. Klein, M. Jansen, Z. Anorg. Allg. Chem. 626 (2000) 136–140.
[24] M.W. Chase, Nist-JANAF Thermochemical Tables, 4th ed., American Chemical Society, American Institute of Physics, National Bureau of Standarts, New York, 1998.
[25] R. Bouaziz, G. Papin, A.-P. Rollet, Compt. Rend. Acad. Sci. Paris Ser. 262 (1966) 1051–1054.
[26] J.L. Henry, S.A. O'Hare, M.P. Krug. U.S. Bur. Mines Topical Rep. USBM-1532, 1971.
[27] J.P. Maupre. Comm. Energ. Atomique Rep. CEA-R-4905, 1978.
[28] J.L. Tallman, J.L. Margrave, J. Inorg. Nucl. Chem. 21 (1961) 40–44.
[29] E.G. Bunzel, E.J. Kohlmeyer, Z. Anorg. Allg. Chem. 254 (1–2) (1947) 1–30.
[30] T.V. Rode, G.A. Golder. Dokl. Akad. Nauk. SSSR110 (1956) 1001–1004.
[31] V.G. Kuznetsov, V.M. Bakulina, S.A. Tokareva, A.N. Zimina, J. Struct. Chem. 5 (1) (1964) 126–128.
[32] G.P. Nikol'skii, Z.A. Bagdasar'yan, I.A. Kazarnovskii, Dokl. Akad. Nauk SSSR 77 (1) (1951) 69–72.
[33] R.L. Eichelberg. U.S. At. Energy Comm. Rep. AI-AEC-12685 (1968).
[34] K.T. Claxton, in: M.H. Cooper (Ed.), Proc. Int. Conf. on Liquid Metal Technol. in Energy Prod., Springfield, 1977, pp. 541–545.
[35] K.T. Claxton. In Junta Energ. Nucl. (Spain), pages Rep. JEN-446, 1979.
[36] J.D. Noden, J. Brit. Nucl. Energy Soc. 12 (1) (1973) 57–62.
[37] J.D. Noden, J. Brit. Nucl. Energy Soc. 12 (1) (1973) 329–331.
[38] J.D. Cox, D.D. Wagman, V.A. Medvedev, CODATA Key Values for Thermodynamics, Hemisphere Publishing Corp, New York, 1989.
[39] O. Knacke, O. Kubaschewski, K. Hesselman, Thermochemical Properties of Inorganic Substances, second ed., Springer-Verlag, Berlin, 1991.
[40] A. Dinsdale, Calphad 15 (1991) 317–425.
[41] NASA-TP-3287. N93-19977, 1993.
[42] E.H.P. Cordfunke, R.J.M. Konings, Thermochemical Data for Reactor Materials and Fission Products, North Holland, Amsterdam, 1990.
[43] R. Guillaumont, T. Fanghänel, J. Fuger, I. Grenthe, V. Neck, D.A. Palmer, M.H. Rand, Update on the chemical thermodynamics of uranium, neptunium, plutonium, americium & technetium, OECD Nuclear Energy Agency, Data Bank, Issy-les-Moulineaux (France), 2003.
[44] D.L. Martin, Proc. Roy. Soc. (London) A254 (1279) (1960) 433.
[45] J.D. Filby, D.L. Martin, Proc. Roy. Soc. (London) 276 (1365) (1963) 187.
[46] D.L. Martin, Phys. Rev. 154 (1967) 571–575.
[47] P.A.G. O' Hare, J. Chem. Phys. 56 (1973) 4513.
[48] G.T. Furukawa. U.S. Nat. Bur. Stand., personal communication, 1967.
[49] R.T. Grimley, J.L. Margrave, J. Chem. Phys. 64 (1960) 1763–1764.
[50] D.R. Fredrickson, M.G. Chasanov, J. Chem. Thermodyn. 5 (4) (1973) 485–490.
[51] L.B. Pankratz. Bull. 672, U.S. Bureau of Mines, 1982.
[52] P.W. Gilles, J.L. Margrave, J. Chem. Phys. 68 (1956) 1333.
[53] S.S. Todd, J. Am. Ceram. Soc. 75 (1953) 1229.
[54] M.C. Chandrasekharaiah, R.T. Grimley, J.L. Margrave, J. Phys. Chem. 63 (1959) 1505.
[55] D.D. Wagman. U.S. Nat. Bur. Stand. Report 7437 ch. B4, 1962.
[56] D.L. Hildenbrand, E. Murad, J. Chem. Phys. 53 (1970) 3403.
[57] R.H. Lamoreaux, D.L. Hildenbrand, J. Phys. Chem. Ref. Data 13 (1984) 151–173.
[58] L.F. Malheiros, C. Chatillon, M. Allibert, High Temp. High Press 20 (1988) 361–378.
[59] D.L. Hildenbrand, K.H. Lau, J. Chem. Phys. 98 (1993) 4076–4081.
[60] O. Beneš, R.J.M. Konings, S. Wurzer, M. Sierig, A. Dockendorf, Thermochimica Acta 509 (1–2) (2010) 62–66.
[61] M. Hillert, B. Jansson, B. Sundman, J. Agren. Metall. Trans. A16 (1) (1985) 261–266.
[62] I. Ansara, B. Sundman, Scientific Group Thermodata Europe, Computer Handling and Determination of Data, North Holland, Amsterdam, 1986.
[63] R.J.M. Konings, O. Beneš, J. Phys. Chem. Ref. Data 39 (2010), 043102.
[64] R.J.M. Konings, O. Beneš, A. Kovacs, D. Manara, D. Sedmidubský, L. Gorokhov, V.S. Iorish, V. Yungman, E. Shenyavskaya, E. Osina, J. Phys. Chem. Ref. Data 43 (1) (2014).
[65] A.L. Smith, P.E. Raison, L. Martel, T. Charpentier, I. Farnan, D. Prieur, C. Hennig, A.C. Scheinost, R.J.M. Konings, A.K. Cheetham, Inorg. Chem. 53 (2014) 375–382.
[66] A.L. Smith, P.E. Raison, L. Martel, D. Prieur, T. Charpentier, G. Wallez, E. Suard, A.C. Scheinost, C. Hennig, P. Martin, K.O. Kvashnina, A.K. Cheetham, R.J.M. Konings, Inorg. Chem. 54 (2015) 3552–3561.
[67] D.J.W. IJdo, S. Akerboom, A. Bontenbal, J. Solid State Chem. 221 (2015) 1–4.
[68] A.L. Smith, J.-Y. Colle, P.E. Raison, O. Beneš, R.J.M. Konings, J. Chem. Thermodyn. 90 (2015) 199–208.
[69] A.L. Smith, Structural and Thermodynamic Properties of Sodium Actinide Ternary Oxides, University of Cambridge, 2015, PhD thesis.
[70] S. Van den Berghe, A. Leenaers, C. Ritter, J. Solid State Chem. 177 (2004) 2231–2236.
[71] E.H.P. Cordfunke, D.J.W. IJdo. J. Solid State Chem. 115 (1995) 299–304.
[72] I.P. Roof, M.D. Smith, H.-C. zur Loye. J. Cryst. Growth 312 (2010) 1240–1243.
[73] A.L. Smith, P. Martin, D. Prieur, A.C. Scheinost, P.E. Raison, A.K. Cheetham, R.J.M. Konings, Inorg. Chem. 55 (4) (2015) 1569–1579.
[74] R. Scholder, H. Gläser, Z. Anorg. Allg. Chem. 327 (1964) 15–27.
[75] S.F. Bartram, R.E. Fryxell, J. Inorg. Nucl. Chem. 32 (1970) 3701–3706.
[76] R. Lorenzelli, T. Athanassiadis, R. Pascard, J. Nucl. Mater. 130 (1985) 298–315.
[77] J.-P. Marcon, O. Pesme, M. Franco, Rev. Int. Hautes Tempér. et Réfract. 9 (1972) 193–196.
[78] S. Pillon, Etude des diagrammes de phases U-O-Na, Pu-O-Na et U, Pu-O-Na, Université Du Languedoc, 1989, PhD thesis.
[79] A.L. Smith, J.-C. Griveau, E. Colineau, P.E. Raison, G. Wallez, R.J.M. Konings, J. Chem. Thermodyn. 91 (2015) 245–255.
[80] I. Grenthe, J. Fuger, R.J.M. Konings, R.J. Lemire, A.B. Muller, C. Nguyen-Trung Cregu, H. Wanner. Chemical Thermodynamics of Uranium. OECD Nuclear Energy Agency, Data Bank, Issy-les-Moulineaux (France), 1992.
[81] E.H.P. Cordfunke, R.P. Muis, W. Ouweltjes, H.E. Flotow, P.A.G. O'Hare, J. Chem. Thermodyn. 14 (1982) 313–322.
[82] D.R. Fredrickson, P.A.G. O'Hare, J. Chem. Thermodyn. 8 (1976) 353–360.
[83] D.W. Osborne, E.F. Howard, J. Chem. Thermodyn. 4 (1972) 411–418.
[84] P.A.G. O'Hare, W.A. Shinn, F.C. Mrazek, A.E. Martin, J. Chem. Thermodyn. 4 (1972) 401–409.
[85] D.R. Fredrickson, M.G. Chasanov, J. Chem. Thermodyn. 4 (1972) 419–423.
[86] J.E. Battles, W.A. Shinn, P.E. Blackburn, J. Chem. Thermodyn. 4 (1972) 425–439.
[87] I. Jayanthi, V.S. Iyer, S.G. Kulkarni, G.A. Rama Rao, V. Venugopal, J. Nucl. Mater. 211 (1994) 168–174.
[88] R. Pankajavalli, V. Chandramouli, S. Anthonysamy, K. Ananthasivan, V. Ganesan, J. Nucl. Mater. 420 (2012) 437–444.
[89] J.L. Fleche, Fleche. Phys. Rev. B65 (2002) 245116.1–245116.10.
[90] S.J. Clark, M.D. Segall, C.J. Pickard, P.J. Hasnip, M.J. Probert, K. Refson, M.C. Payne, Zeitschrift für Kristallographie 220 (5–6) (2005) 567–570.
[91] D. Vanderbilt, Phys. Rev. B 41 (1990) 7892.
[92] J.P. Perdew, K. Burke, M. Ernzerhof, Phys. Rev. Lett. 77 (1996) 3865–3868.
[93] J.D. Pack, H.J. Monkhorst, Phys. Rev. B 16 (1977) 1748.
[94] R.C. Weast (Ed.). CRC Handbook of Chemistry and Physics, 69 ed., CRC Press, Florida.
[95] P. Zeller. Private communication, DEN-Service de la Corrosion et du Comportement des Matériaux dans leur Environnement (SCCME), CEA, Université Paris-Saclay, F-91191 Gif-sur-Yvette cedex, France.
[96] T.B. Douglas, J. Research Natl. Bur. Standards 52 (1954) 223–226.
[97] F.A. Rough, A.A. Bauer. Technical report, 1958.
[98] R.J.M. Konings, O. Benes, J.-C. Griveau. In Comprehensive Nuclear Materials, Vol. 2, Chapter 2.01: The Actinides Elements: Properties and Characteristics, (2012) 1–20.
[99] C. Guéneau, M. Baichi, D. Labroche, C. Chatillon, B. Sundman, J. Nucl. Mater. 304 (2002) 161–175.
[100] G.L. Hofman, J.H. Bottcher, J.A. Buzzell, G.M. Schwartzenberger, J. Nucl. Mater. 139 (1986) 151–155.
[101] W.G. Lyon, D.W. Osborne, H.E. Flotow, H.R. Hoekstra, J. Chem. Thermodyn. 9 (1977) 201–210.
[102] K. Popa, E. Colineau, F. Wastin, R.J.M. Konings, J. Chem. Thermodyn. 39 (2007) 104–107.
[103] R.J.M. Konings, K. Popa, E. Colineau, F. Wastin, J. Chem. Thermodyn. 40 (2008) 220–224.
[104] A.L. Smith, J.-C. Griveau, E. Colineau, P.E. Raison, R.J.M. Konings, Thermochimica Acta 617 (2015) 129–135.
[105] R.J.M. Konings, A.L. Smith. Unpublished results, 2016.
[106] H. Kleykamp, KfK 4701 (1990) 31.
[107] D.L. Smith, Nucl. Technol. 20 (1973) 190–199.